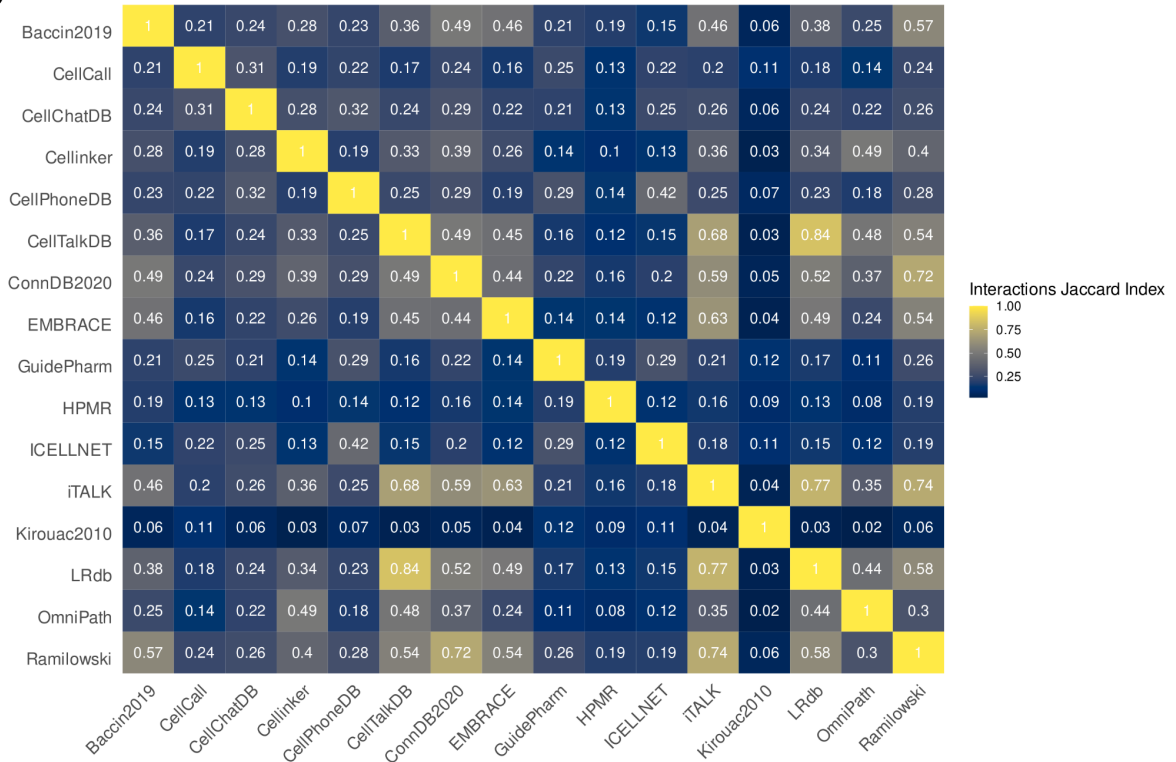


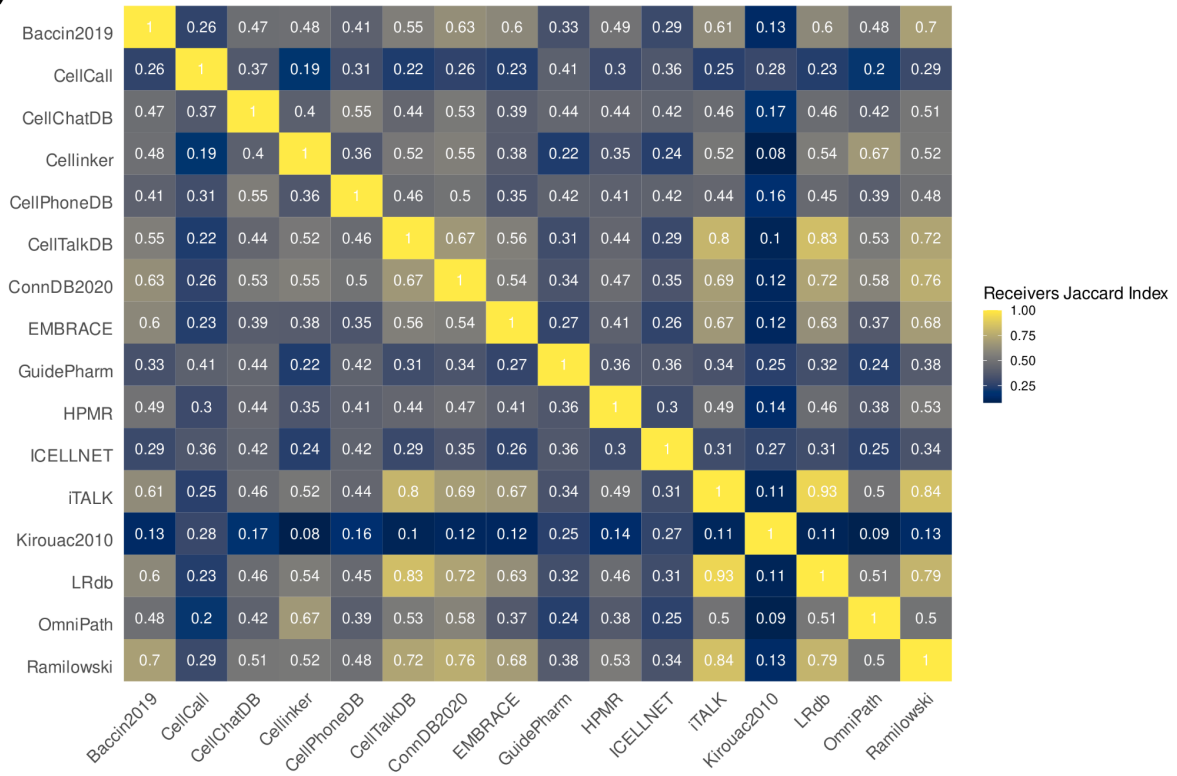
Supplementary Information

Supplementary Figure S1. *Overlap between the resources represented as Jaccard indices between A) Interactions B) Receivers and C) Transmitters from different resources.*

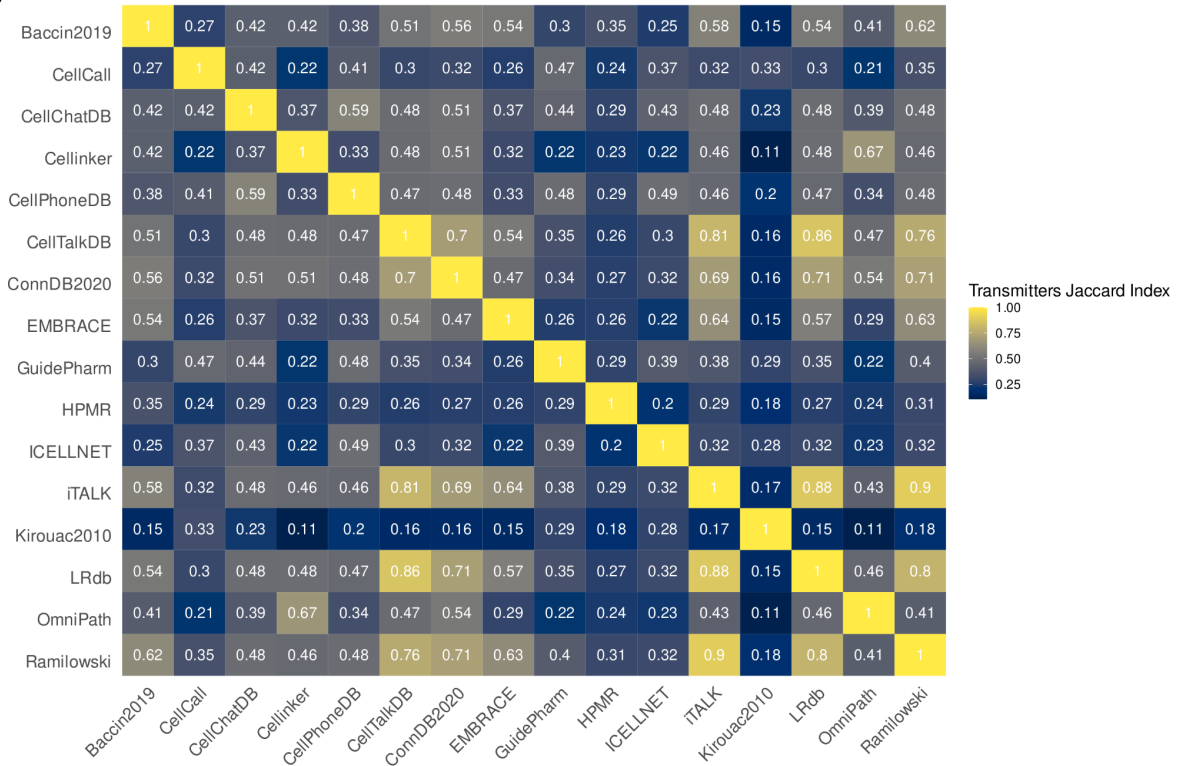
A)



B)

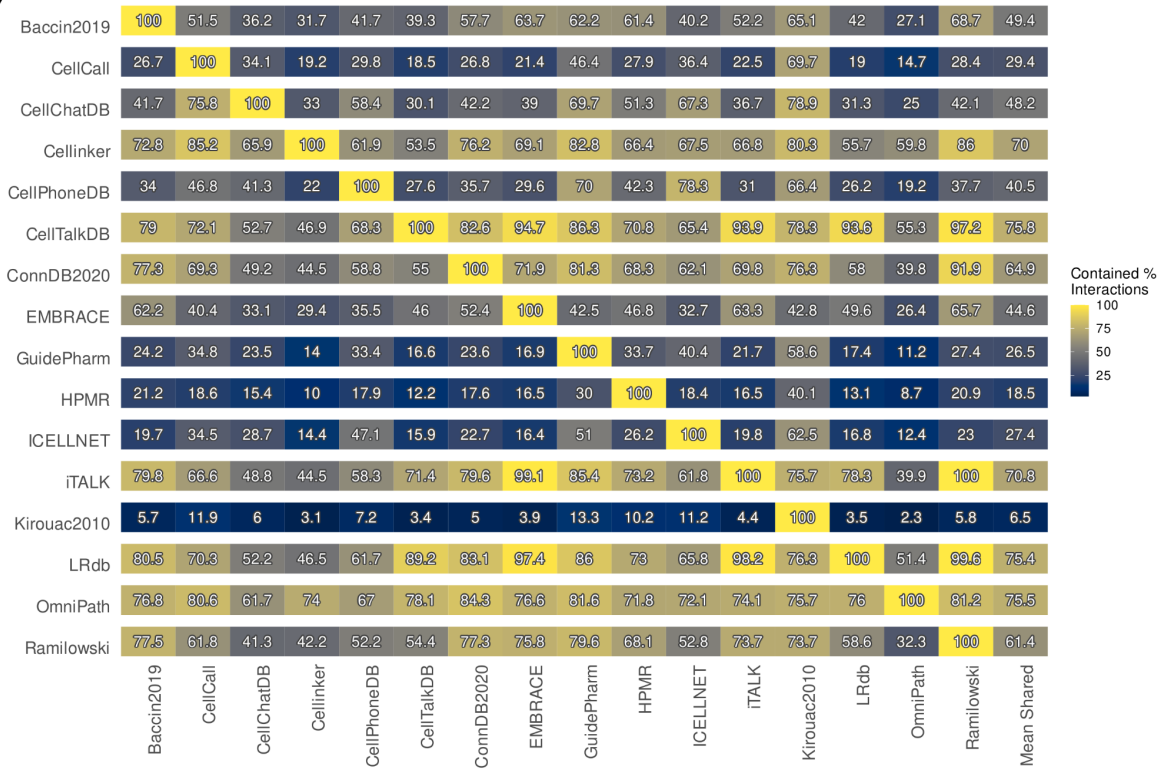


C)

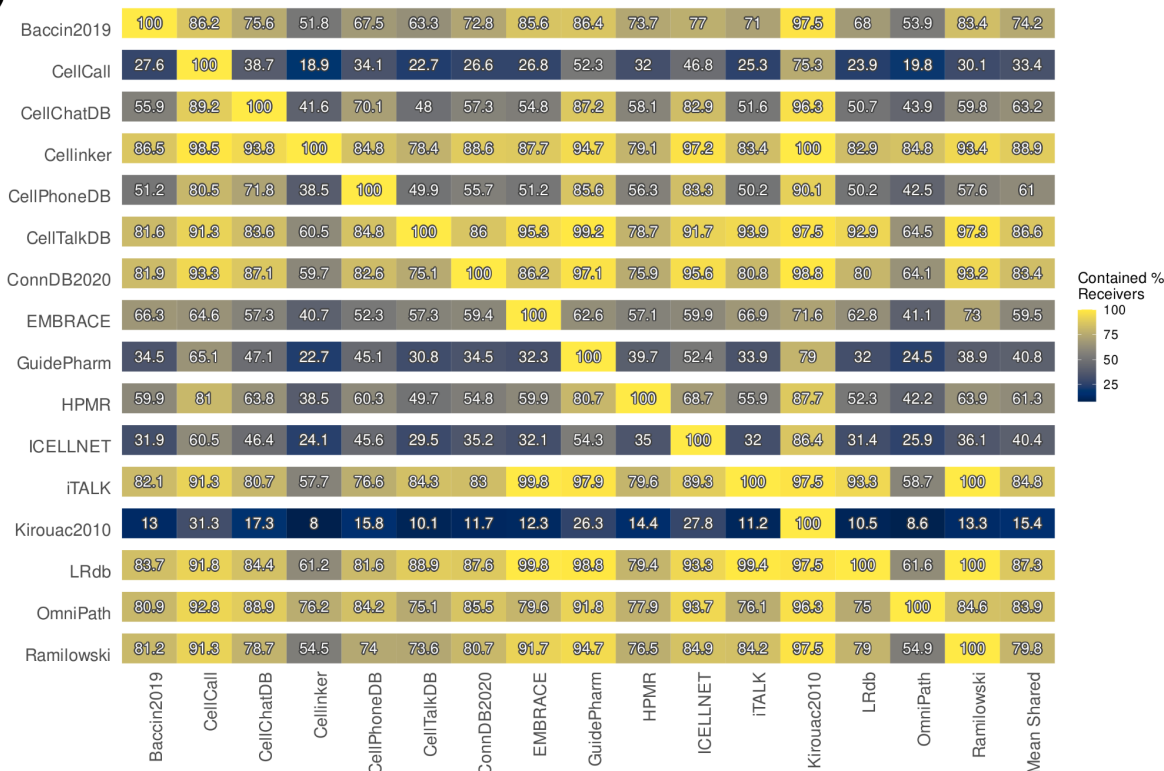


Supplementary Figure S2. Asymmetric overlap between the resources. A) Interactions B) Receivers, C) Transmitters, and D) Curated interactions present in each resource when taken from the rest of the resources. Note these plots are asymmetric and represent the % of interactions from the resources on the X axis found in each resource on the Y axis.

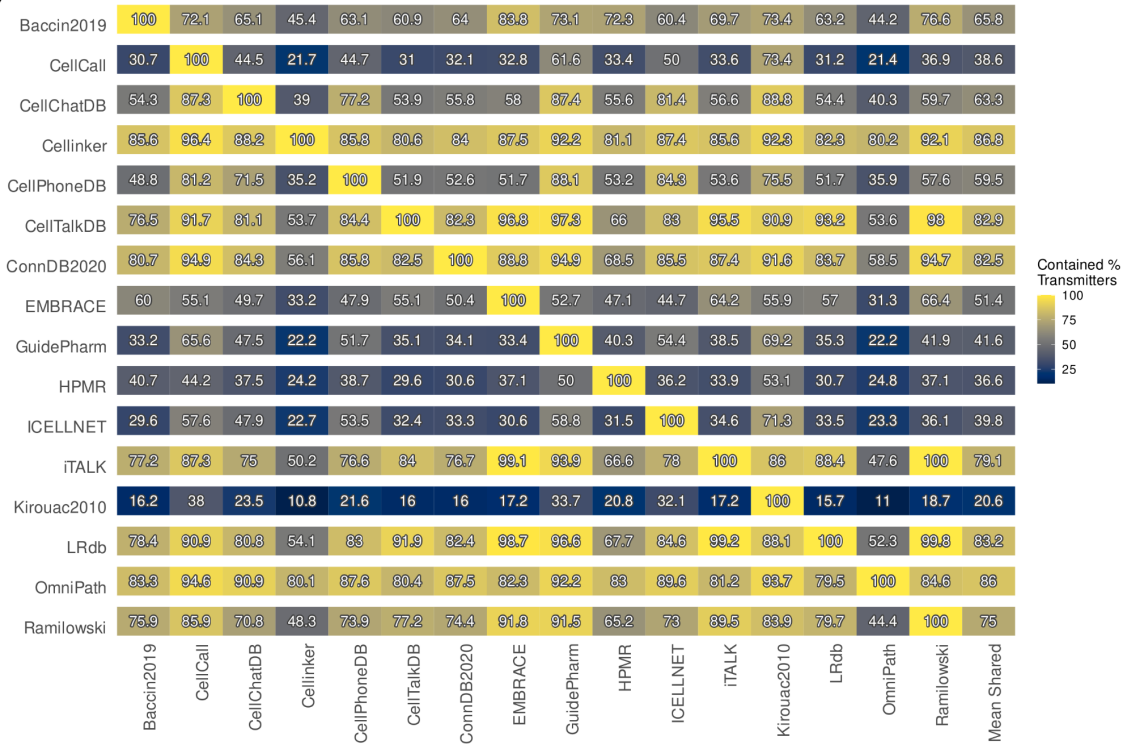
A)



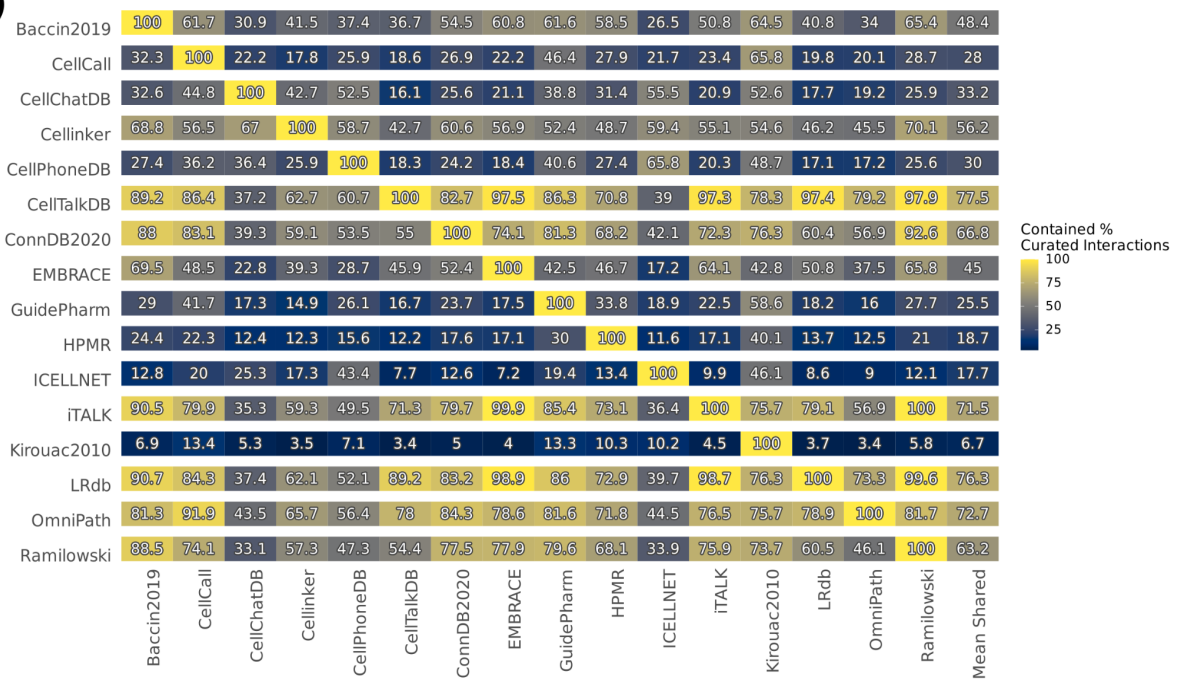
B)



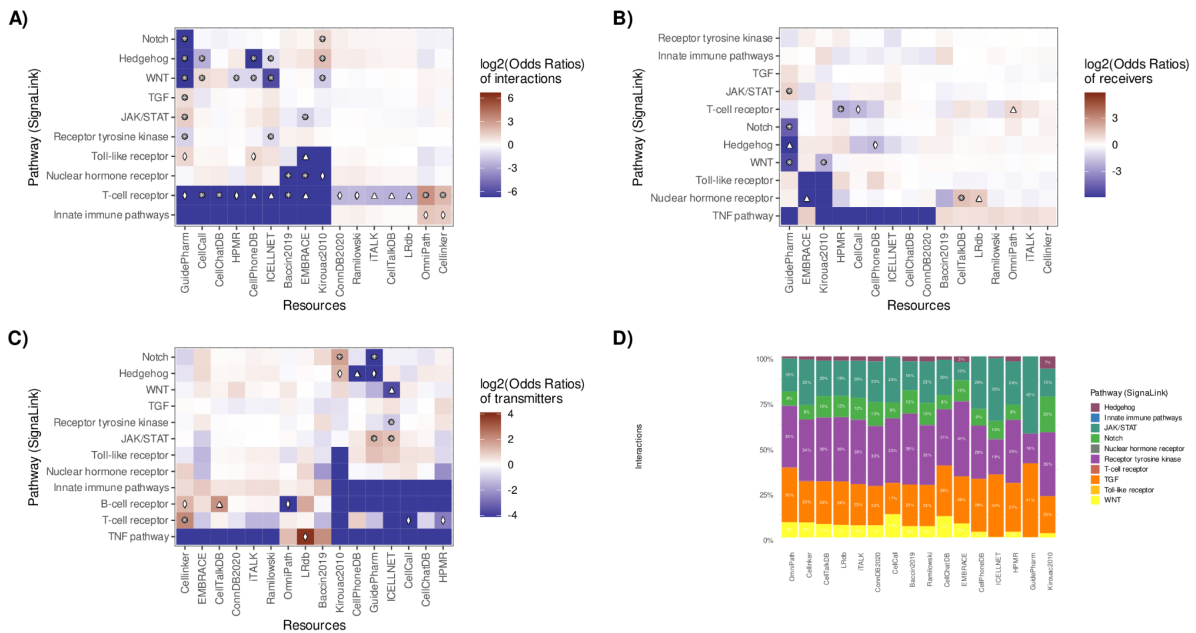
C)



D)

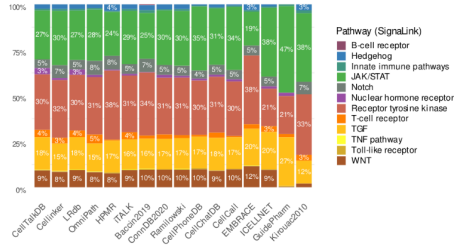


Supplementary Figure S3. *Signalink* pathway distributions across CCC resources. Enrichment Scores (A-C), Percentage Proportions (D-F), and Number of matches (G-I) to the *Signalink* database per resource for Interactions, Receivers and Transmitters from different CCC resources. Fisher's exact test was used to estimate the differentially-represented categories. Differentially represented (absolute(log2(Odds ratio)) > 1) categories were marked according to FDR-corrected *p*-values =< 0.05 (diamond; \diamond), 0.01 (triangle; \triangle), and 0.001 (8-pointed asterisk; *).



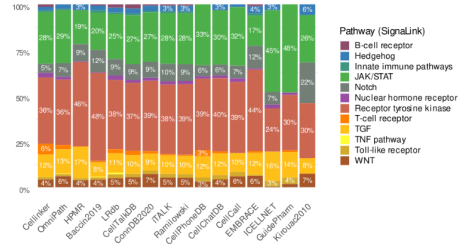
E)

Receivers



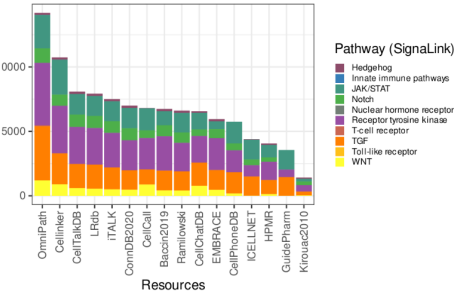
F)

Transmitters



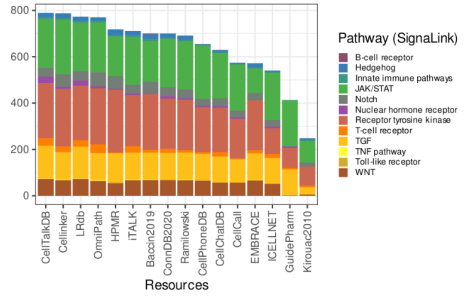
G)

Interactions



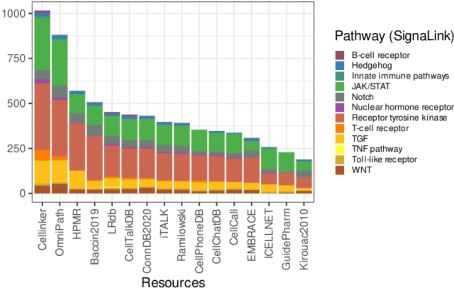
H)

Receivers

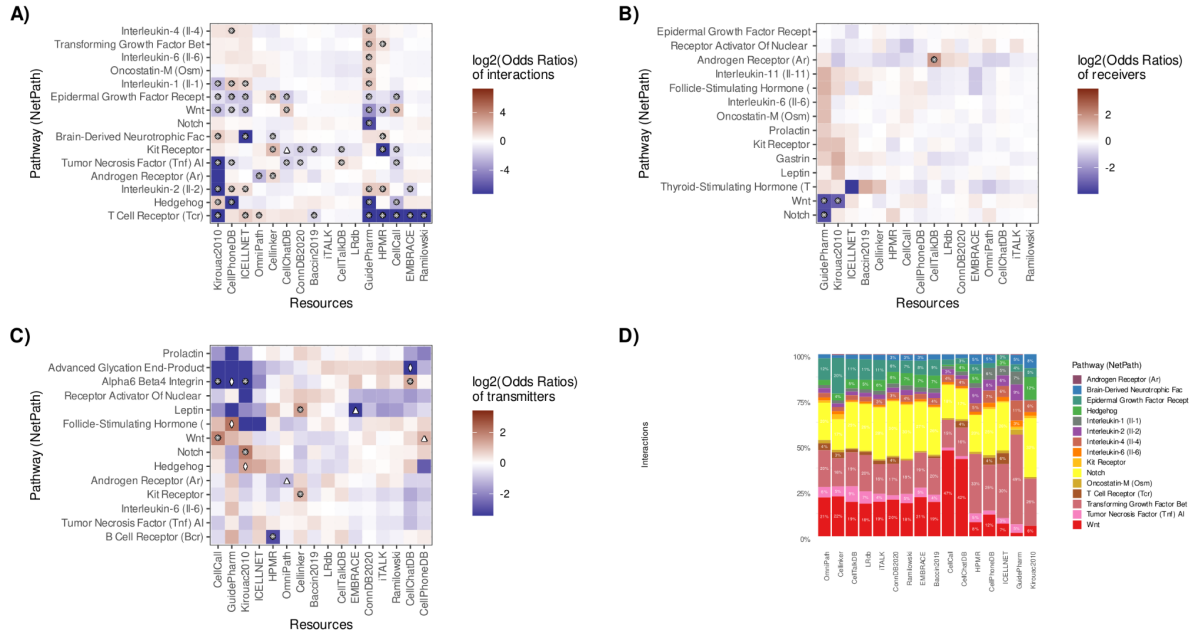


I)

Transmitters

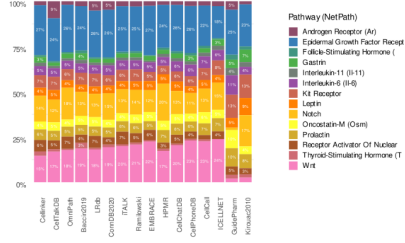


Supplementary Figure S4. NetPath pathway distributions across CCC resources. Enrichment Scores (A-C), Percentage Proportions (D-F), and Number of matches (G-I) to the NetPath database per resource for Interactions, Receivers and Transmitters from different CCC resources. Fisher's exact test was used to estimate the differentially-represented categories. Differentially represented ($|\text{absolute}(\log_2(\text{Odds ratio})) > 1$) categories were marked according to FDR-corrected p -values $= < 0.05$ (diamond; \diamond), 0.01 (triangle; \triangle), and 0.001 (8-pointed asterisk; $*$).



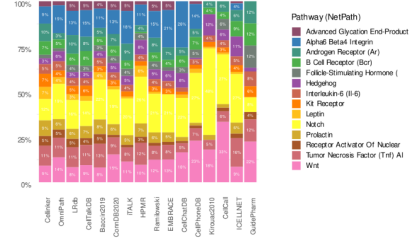
E)

Receivers



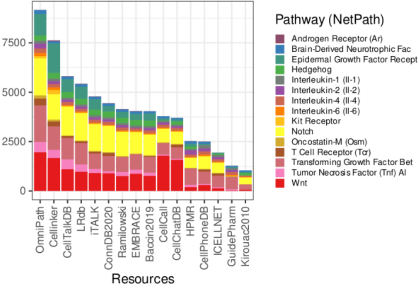
F)

Transmitters



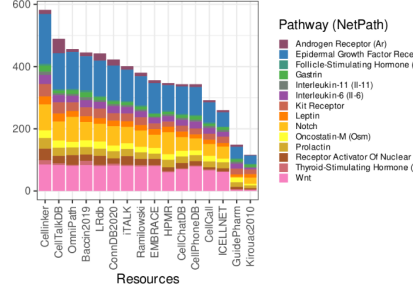
G)

Interactions



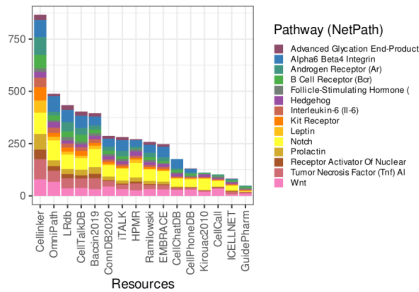
H)

Receivers

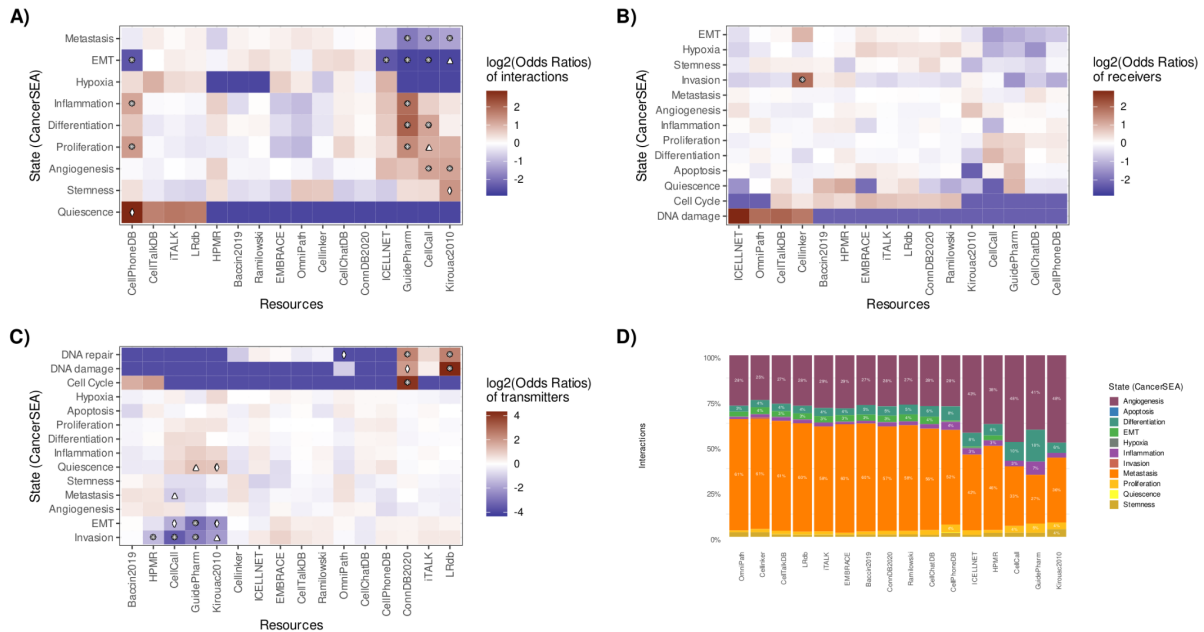


I)

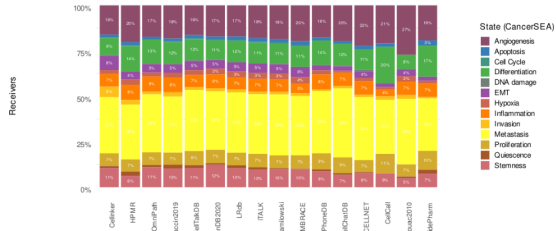
Transmitters



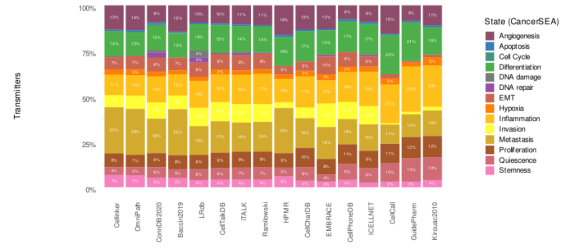
Supplementary Figure S5. CancerSEA cancer genes-set distributions across CCC resources. Enrichment Scores (A-C), Percentage Proportions (D-F), and Number of matches (G-I) to the CancerSEA database per resource for Interactions, Receivers and Transmitters from different CCC resources. Fisher's exact test was used to estimate the differentially-represented categories. Differentially represented (absolute(log2(Odds ratio)) > 1) categories were marked according to FDR-corrected p -values ≤ 0.05 (diamond; \diamond), 0.01 (triangle; \triangle), and 0.001 (8-pointed asterisk; $*$).



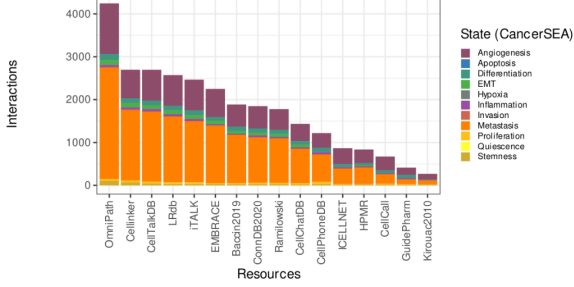
E)



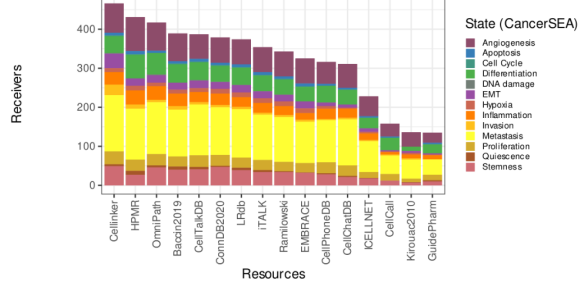
F)



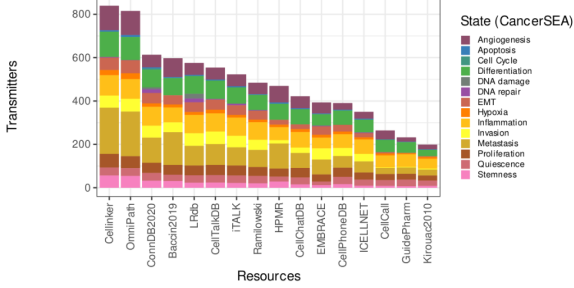
G)



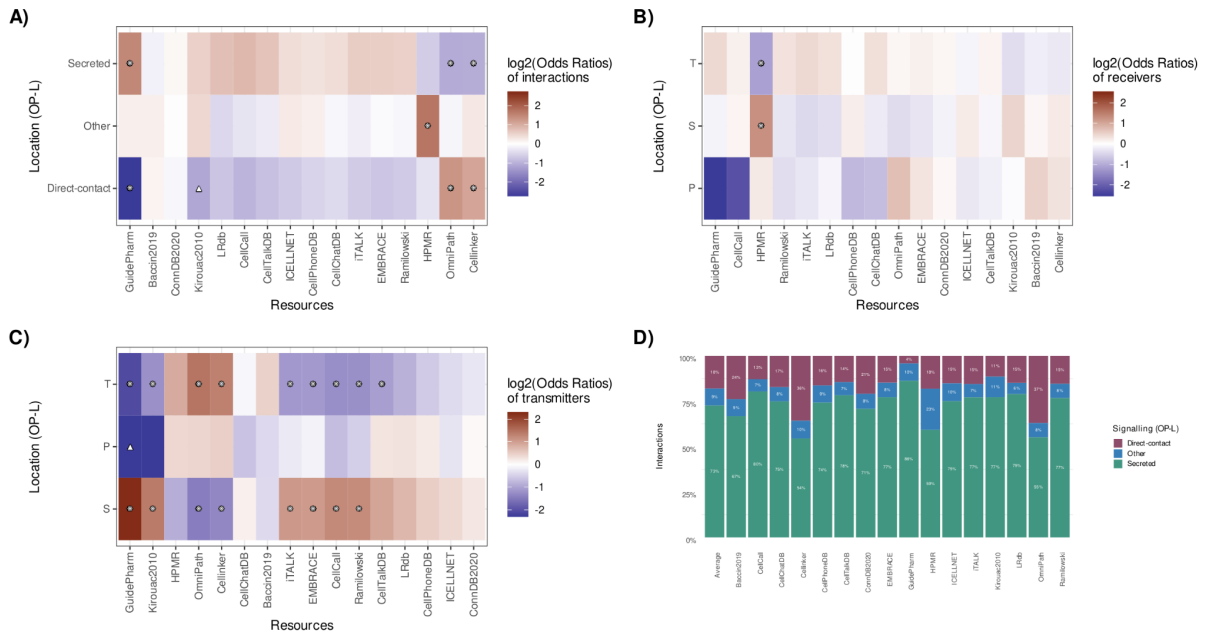
H)

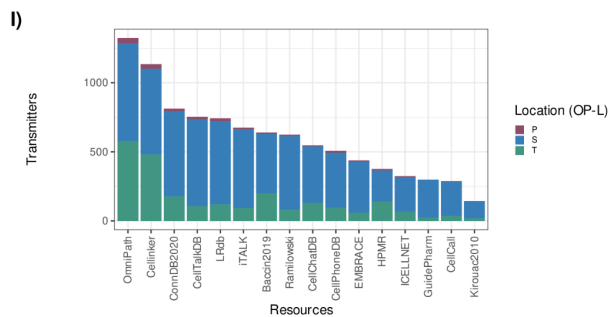
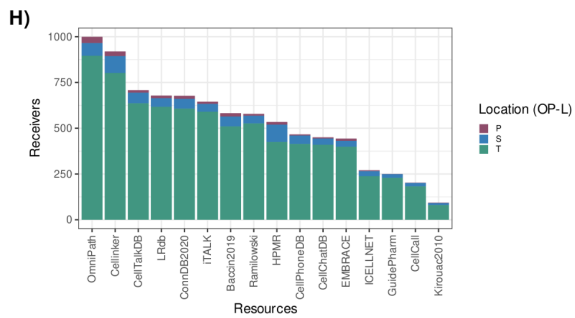
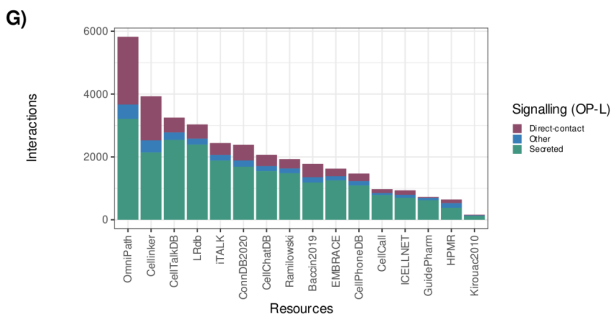
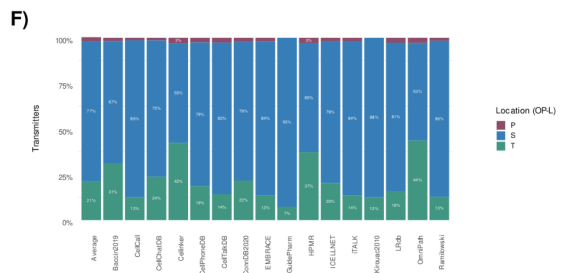
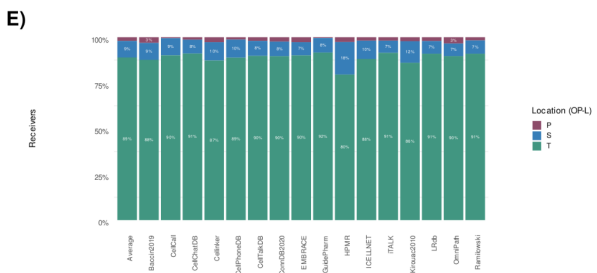


I)

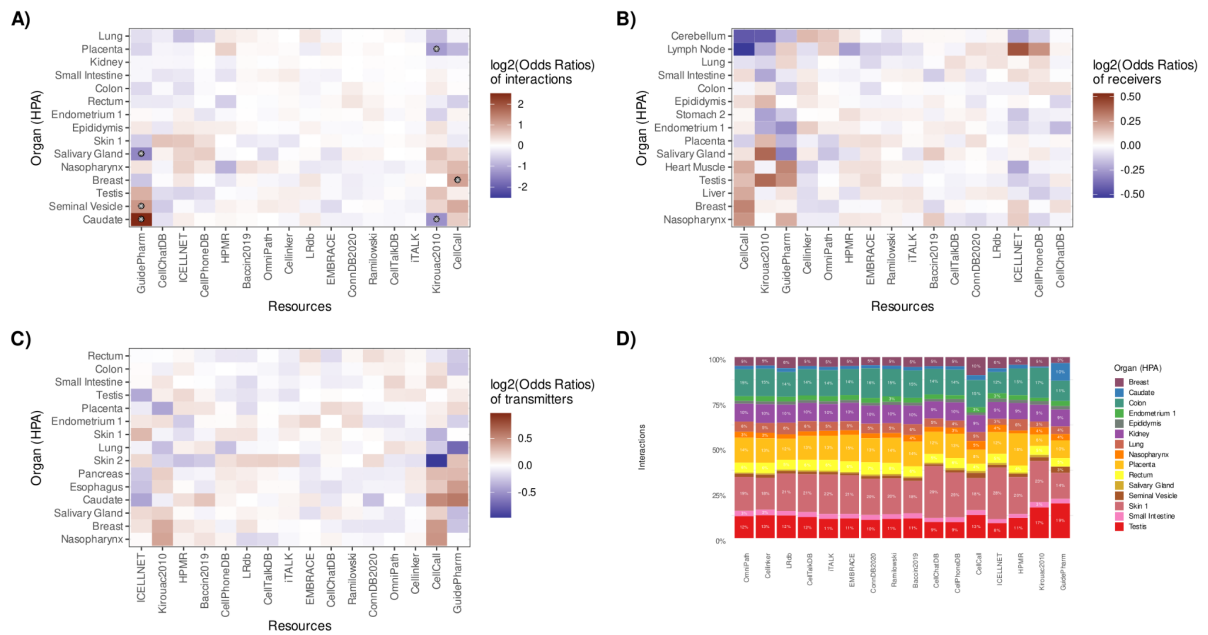


Supplementary Figure S6. Localisation category distributions across CCC resources. Enrichment Scores (A-C), Percentage Proportions (D-F), and Number of matches (G-I) to the subcellular protein localisation categories from the OmniPath database for Interactions, Receivers and Transmitters from different CCC resources. ‘T’, ‘P’, and ‘S’ stand for transmembrane, peripheral, and secreted, respectively. Fisher's exact test was used to estimate the differentially-represented categories. Differentially represented ($|\text{absolute}(\log_2(\text{Odds ratio})) > 1$) categories were marked according to FDR-corrected p -values ≤ 0.05 (diamond; \diamond), 0.01 (triangle; \triangle), and 0.001 (8-pointed asterisk; $*$).

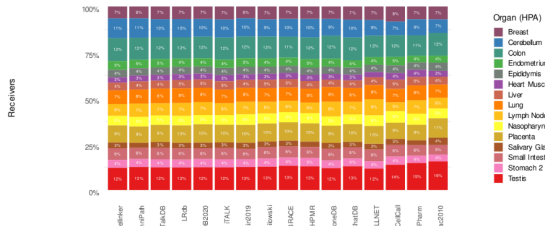




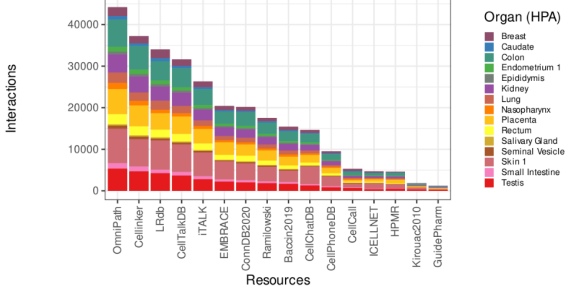
Supplementary Figure S7. Organ-enriched protein distributions across CCC resources. Enrichment Scores (A-C), Percentage Proportions (D-F), and Number of matches (G-I) to the 15 largest categories of organ-enriched proteins in the HPA database per resource for Interactions, Receivers and Transmitters from different CCC resources. Fisher's exact test was used to estimate the differentially-represented categories. Differentially represented (absolute(log2(Odds ratio)) > 1) categories were marked according to FDR-corrected p -values ≤ 0.05 (diamond; \diamond), 0.01 (triangle; \triangle), and 0.001 (8-pointed asterisk; $*$).



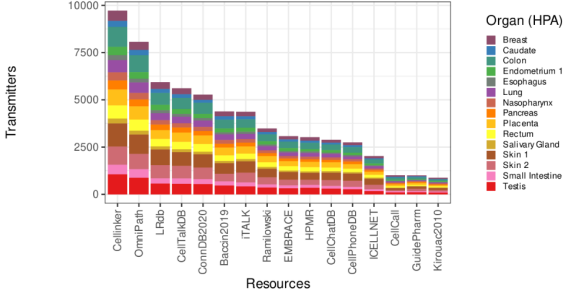
E)



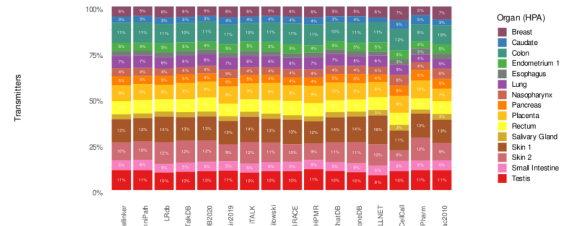
G)



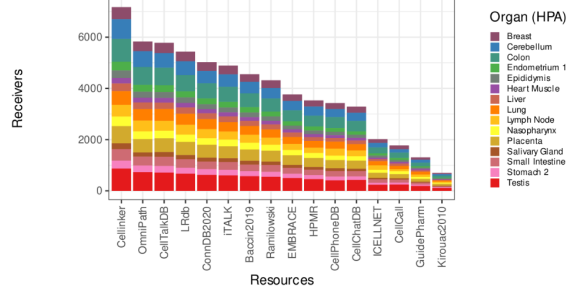
I)



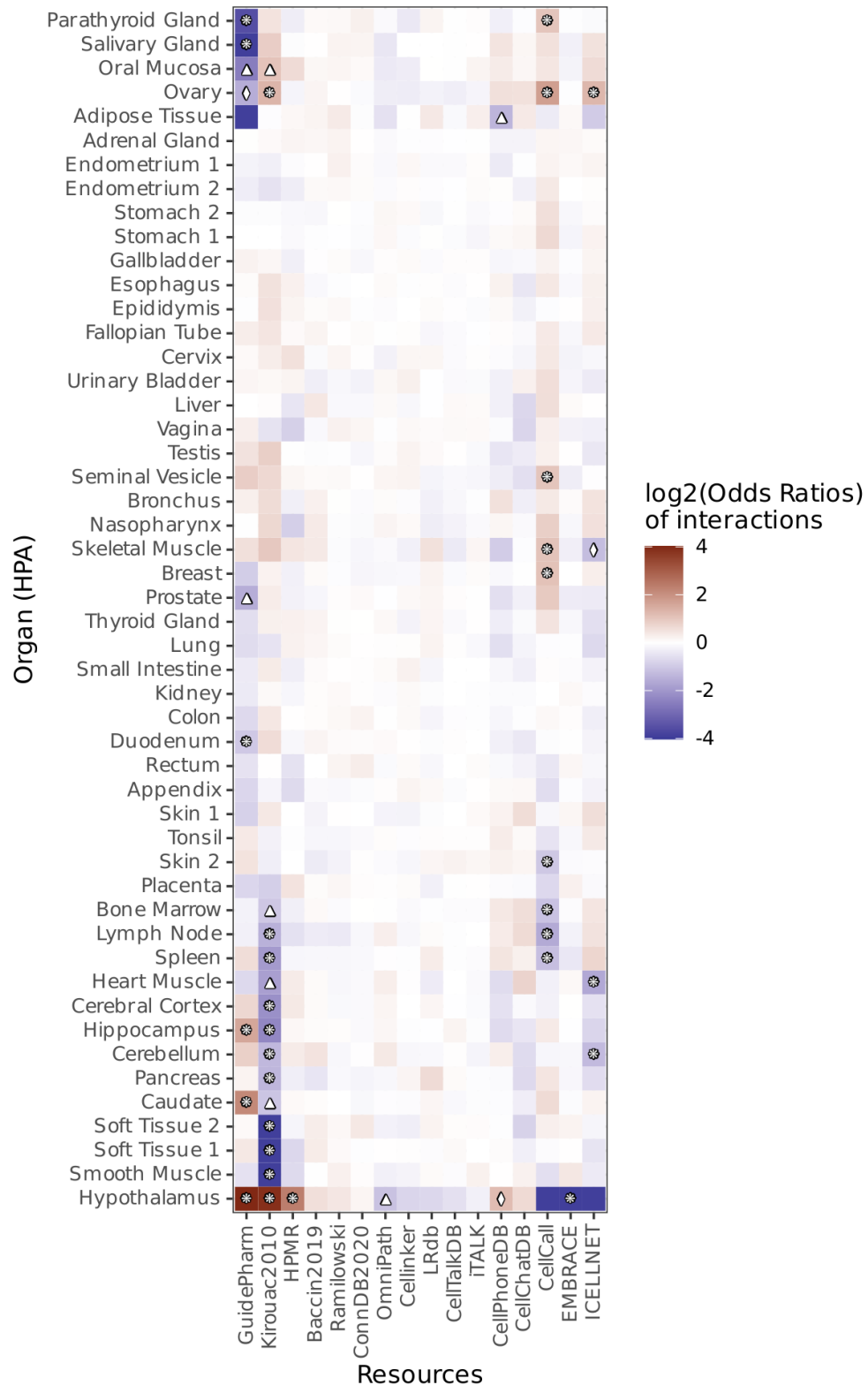
F)



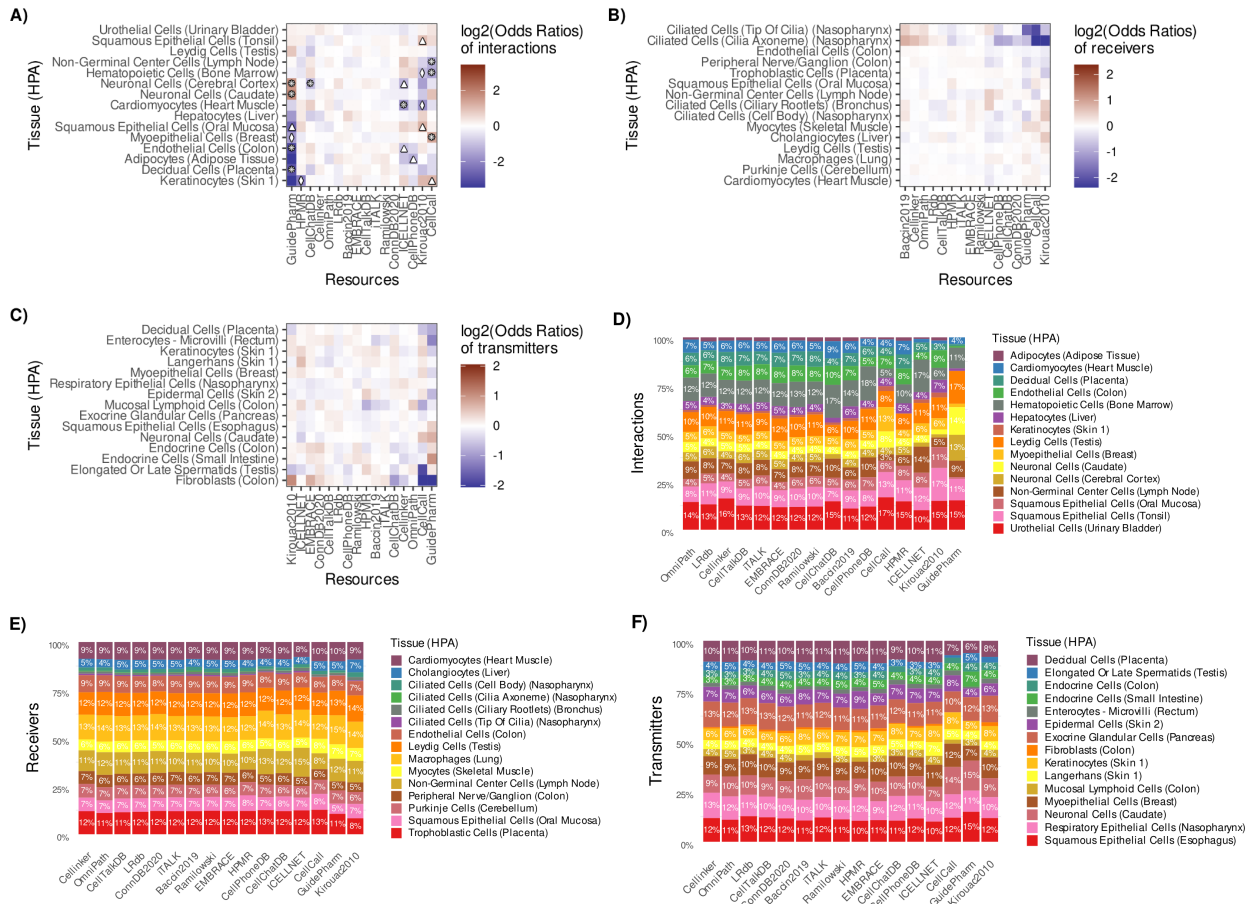
H)



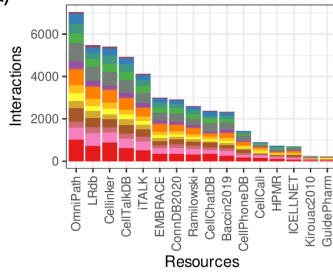
Supplementary Figure S8. Interaction enrichment scores calculated for the largest 50 categories matched to organ-enriched proteins from the HPA database. Fisher's exact test was used to estimate the differentially-represented categories. Differentially represented ($\text{absolute}(\log_2(\text{Odds ratio})) > 1$) categories were marked according to FDR-corrected p -values ≤ 0.05 (diamond; \diamond), 0.01 (triangle; \triangle), and 0.001 (8-pointed asterisk; $*$).



Supplementary Figure S9. Tissue-enriched protein distributions across CCC resources. Enrichment Scores (A-C), Percentage Proportions (D-F), and Number of matches (G-I) to the 15 largest categories of tissue-enriched proteins in the HPA database per resource for Interactions, Receivers and Transmitters from different CCC resources. Fisher's exact test was used to estimate the differentially-represented categories. Differentially represented ($|\log_2(\text{Odds ratio})| > 1$) categories were marked according to FDR-corrected p -values ≤ 0.05 (diamond; \diamond), 0.01 (triangle; \triangle), and 0.001 (8-pointed asterisk; $*$).



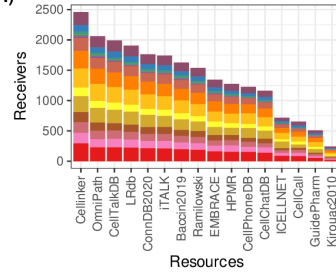
G)



Tissue (HPA)

- Adipocytes (Adipose Tissue)
- Cardiomyocytes (Heart Muscle)
- Decidual Cells (Placenta)
- Endothelial Cells (Colon)
- Hematopoietic Cells (Bone Marrow)
- Hepatocytes (Liver)
- Keratinocytes (Skin 1)
- Leydig Cells (Testis)
- Myoepithelial Cells (Breast)
- Neuronal Cells (Caudate)
- Neuronal Cells (Cerebral Cortex)
- Non-Germinal Center Cells (Lymph Node)
- Squamous Epithelial Cells (Oral Mucosa)
- Urothelial Cells (Urinary Bladder)

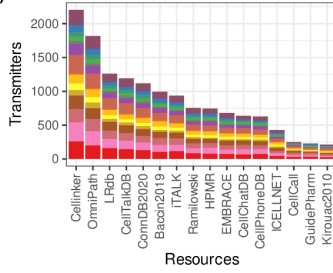
H)



Tissue (HPA)

- Cardiomyocytes (Heart Muscle)
- Cholangiocytes (Liver)
- Ciliated Cells (Cell Body) (Nasopharynx)
- Ciliated Cells (Cilia Axoneme) (Nasopharynx)
- Ciliated Cells (Ciliary Rootlets) (Bronchus)
- Ciliated Cells (Tip Of Cilia) (Nasopharynx)
- Endothelial Cells (Colon)
- Leydig Cells (Testis)
- Macrophages (Lung)
- Myocytes (Skeletal Muscle)
- Non-Germinal Center Cells (Lymph Node)
- Peripheral Nerve/Ganglion (Colon)
- Purkinje Cells (Cerebellum)
- Squamous Epithelial Cells (Oral Mucosa)
- Trophoblastic Cells (Placenta)

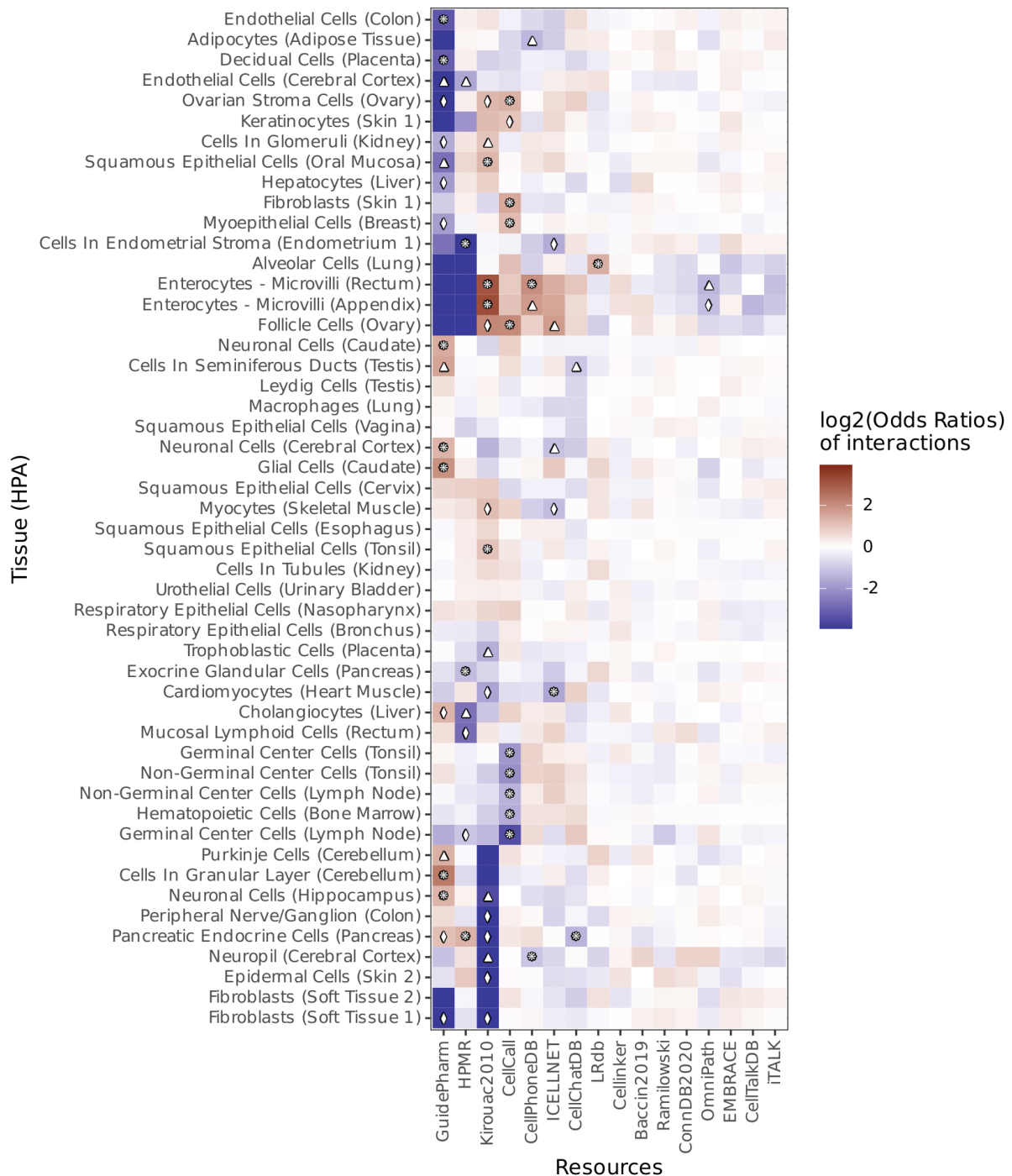
I)



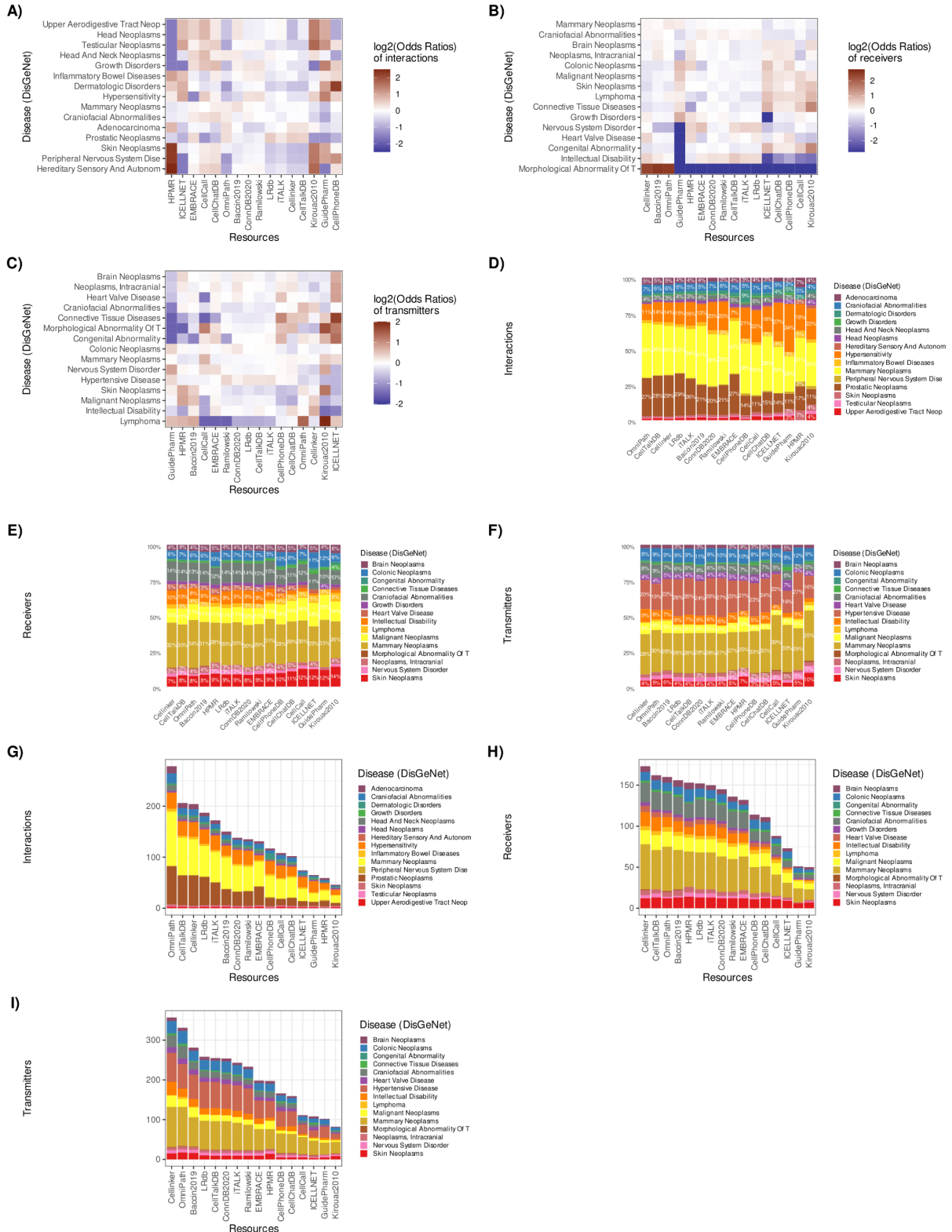
Tissue (HPA)

- Decidual Cells (Placenta)
- Elongated Or Late Spermatis (Testis)
- Endocrine Cells (Colon)
- Endocrine Cells (Small Intestine)
- Enterocytes - Microvilli (Rectum)
- Epidermal Cells (Skin 2)
- Exocrine Glandular Cells (Pancreas)
- Fibroblasts (Colon)
- Keratinocytes (Skin 1)
- Langerhans (Skin 1)
- Mucosal Lymphoid Cells (Colon)
- Myoepithelial Cells (Breast)
- Neuronal Cells (Caudate)
- Respiratory Epithelial Cells (Nasopharynx)
- Squamous Epithelial Cells (Esophagus)

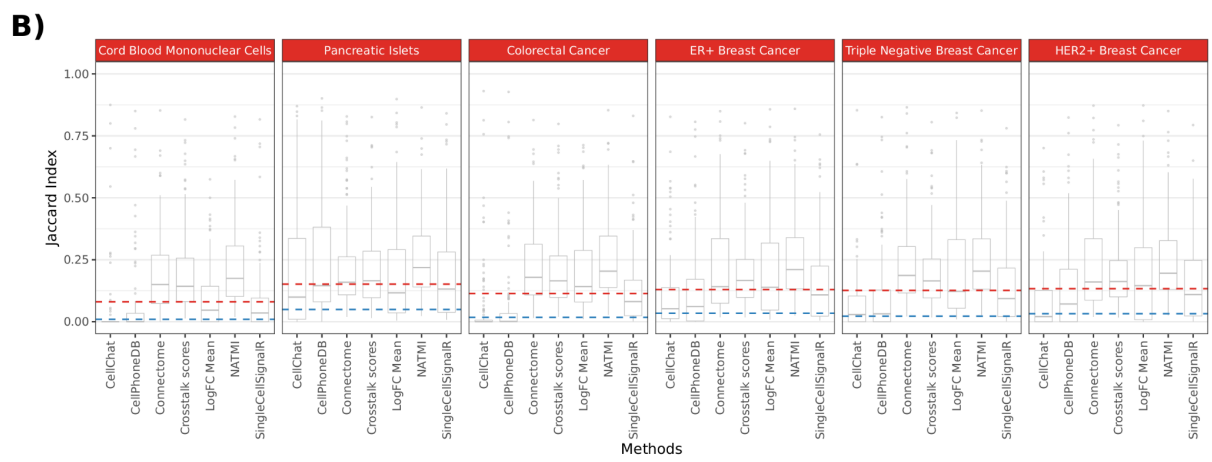
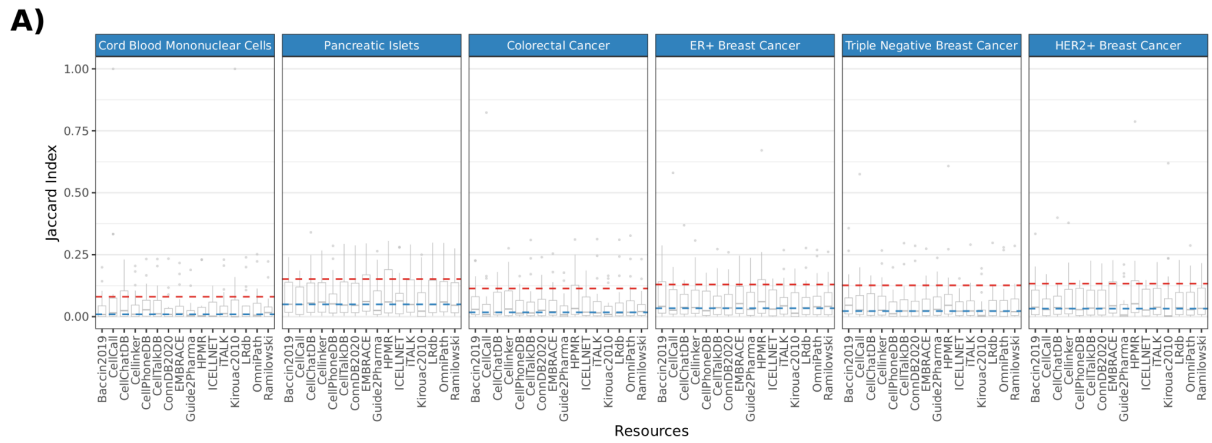
Supplementary Figure S10. Interaction enrichment scores calculated for the largest 50 categories matched to tissue-enriched proteins from the HPA database. Fisher's exact test was used to estimate the differentially-represented categories. Differentially represented ($\text{absolute}(\log_2(\text{Odds ratio})) > 1$) categories were marked according to FDR-corrected p -values ≤ 0.05 (diamond; \diamond), 0.01 (triangle; \triangle), and 0.001 (8-pointed asterisk; $*$).



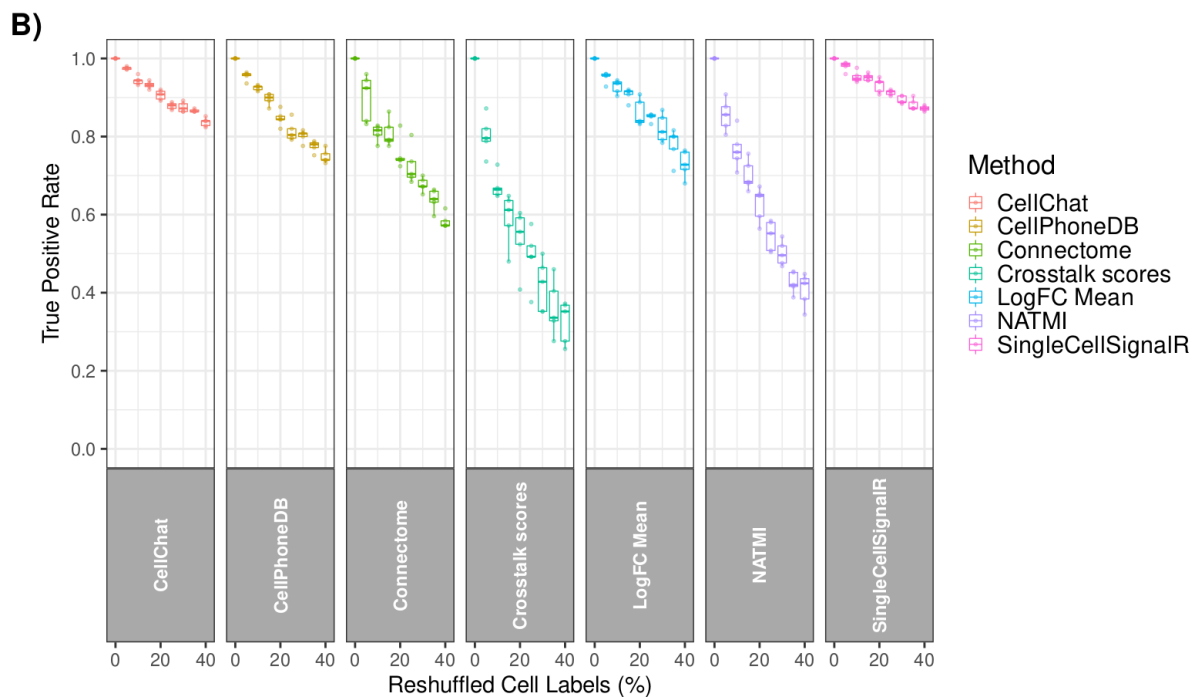
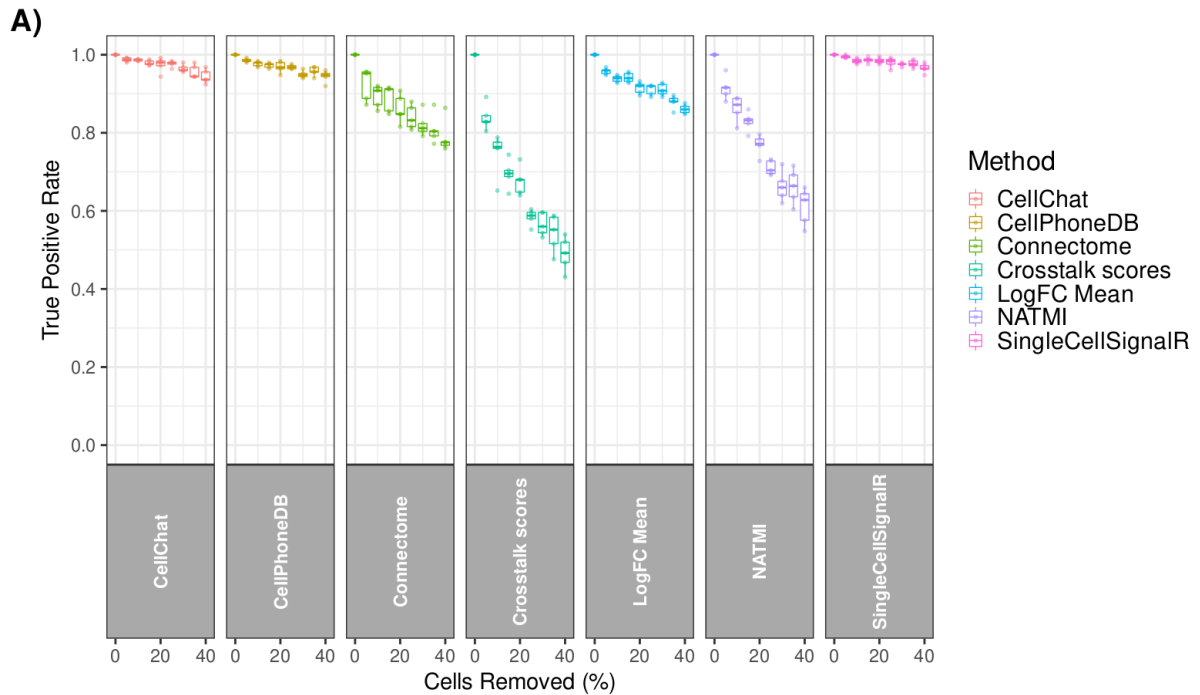
Supplementary Figure S11. Disease-associated gene distributions across CCC resources. Enrichment Scores (A-C), Percentage Proportions (D-F), and Number of matches (G-I) to the DisGeNet database per resource for Interactions, Receivers and Transmitters from different CCC resources. Fisher's exact test was used to estimate the differentially-represented categories. No significant differentially-represented categories were detected following FDR correction.

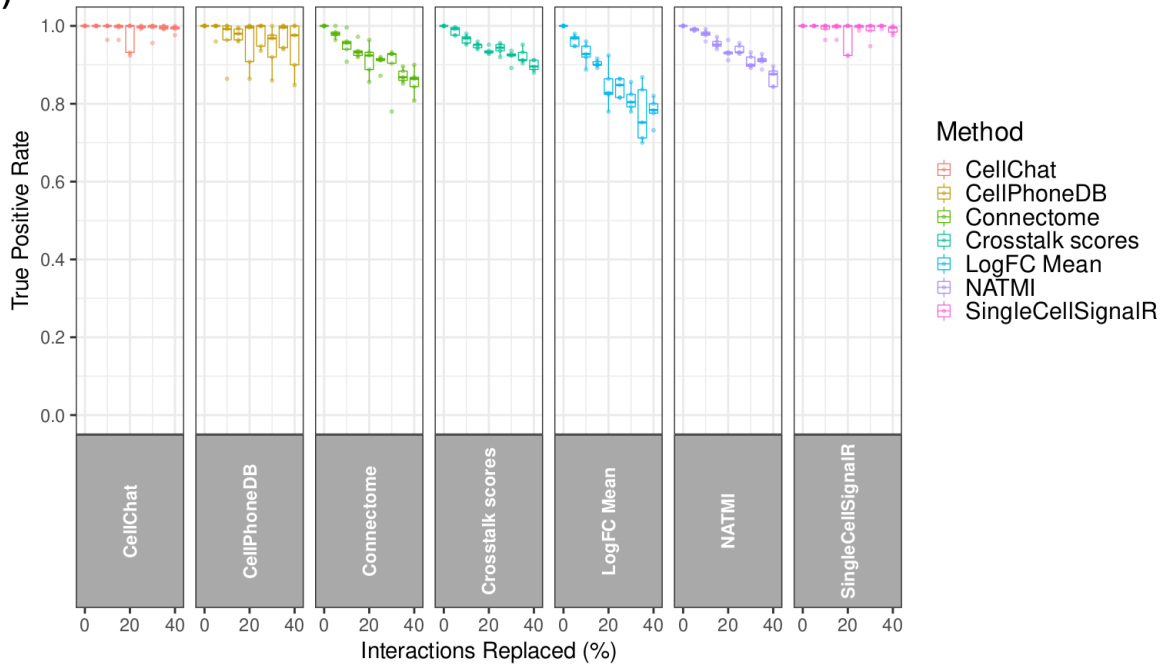
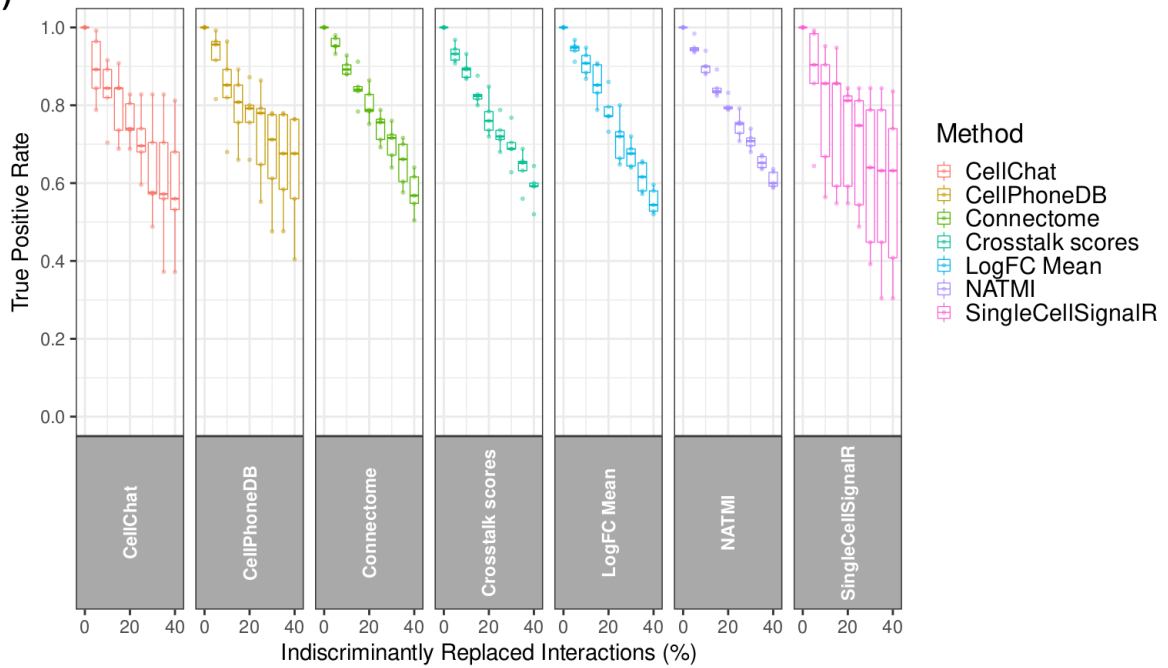


Supplementary Figure S12. Overlap (Jaccard index) in the 1% highest ranked interactions A) when using the same Resource with different Methods (Blue; n=7) and B) when using the same Method with different Resources (Red; n=16). Boxplots represent the median pairwise jaccard index with hinges showing the first and third quartiles and whiskers extending 1.5 above and below the interquartile range.

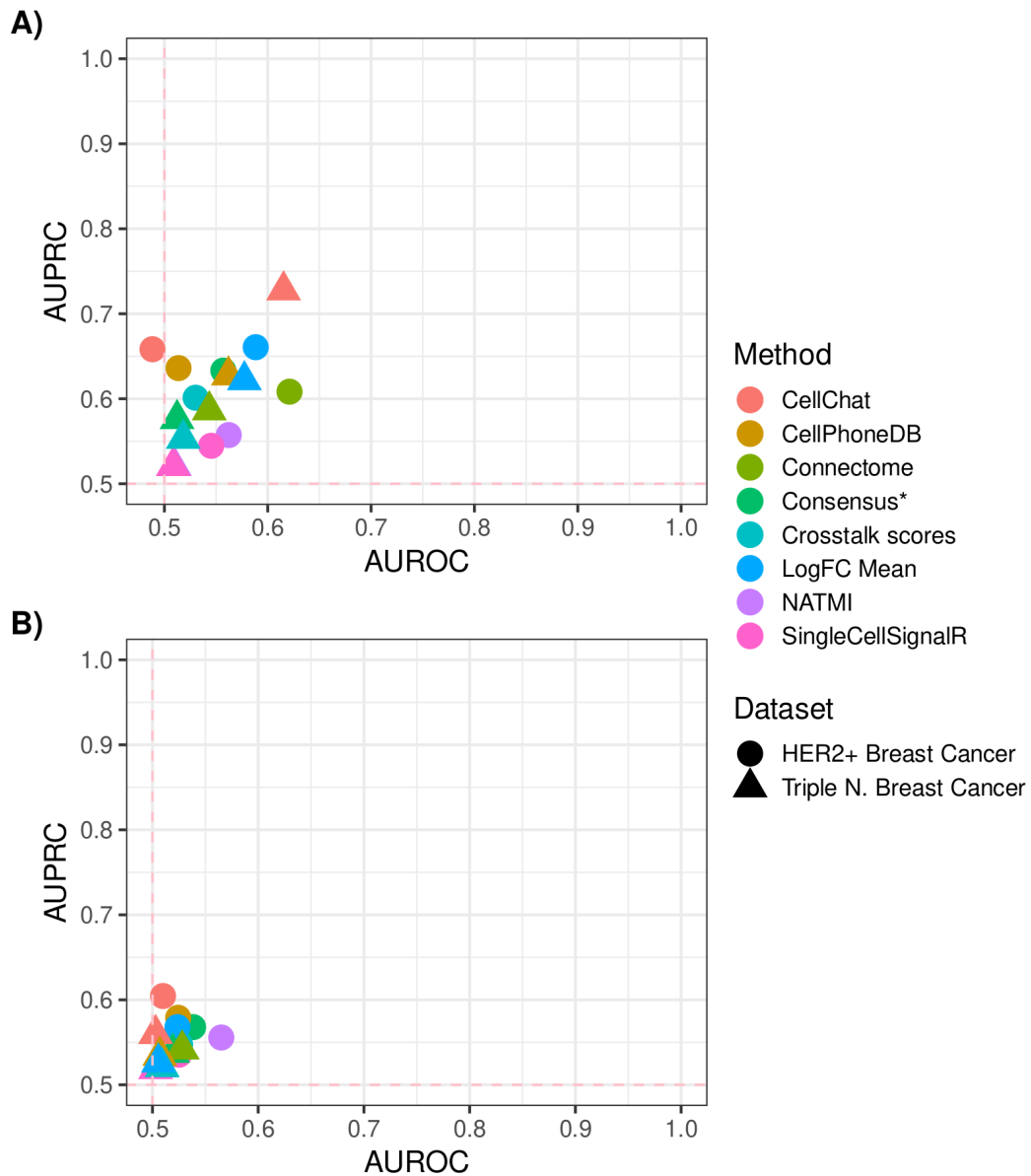


Supplementary Figure S13. Robustness of cell-cell communication predictions to A) Cell type subsampling, B) Reshuffling of cell types labels C) Selective, and D) Non-selective replacement of interactions with putatively false ones. The non-modified predictions (0% modifications) from each method were used to calculate the True Positive Rate. Boxplots represent the median true positive rate with hinges showing the first and third quartiles and whiskers extending 1.5 above and below the interquartile range ($n = 5$).

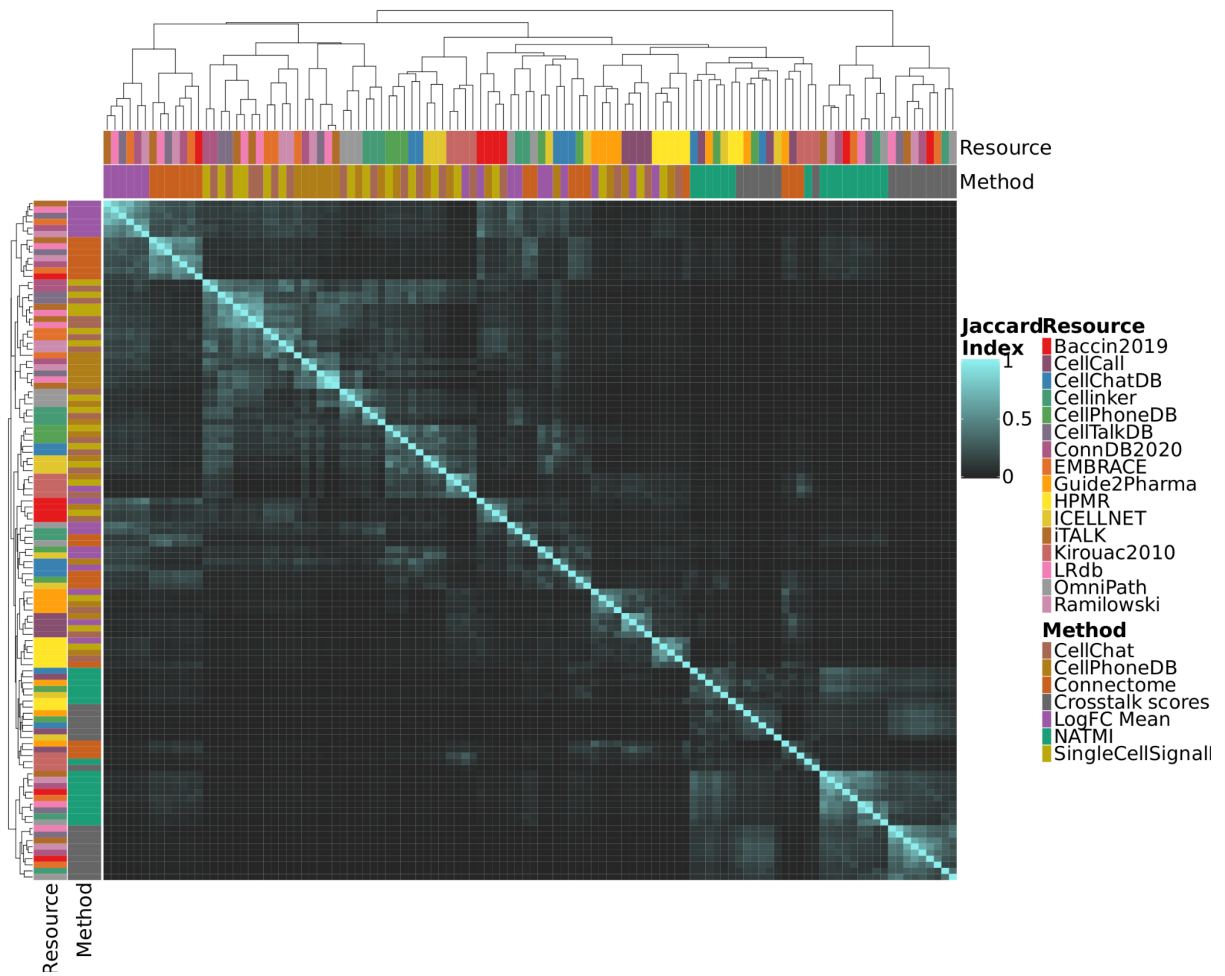


C)**D)**

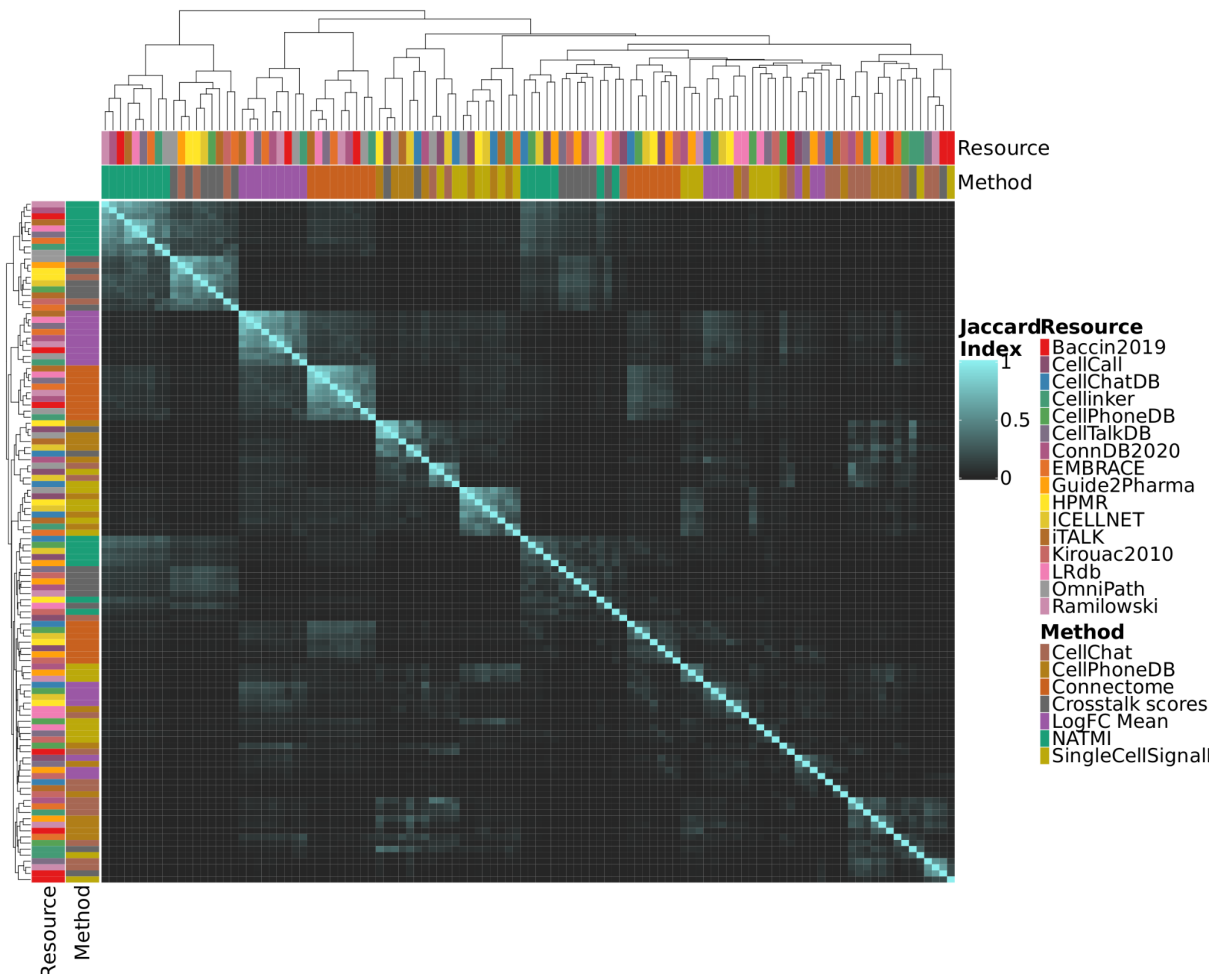
Supplementary Figure S14. AUROC/AUPRC of CCC Method Agreement with Cytokine Activities. A) Each method's performance was estimated independently, i.e. only using the interactions predicted following the preprocessing steps of each method. B) Methods were evaluated using the union of all interactions predictions, and missing interactions were max-imputed. To ameliorate the differences of predictions assigned to the negative class between the different methods, we included a subsampling step, in which we downsampled the negative class 100 times to match the (lower) number of interactions assigned to the positive class.



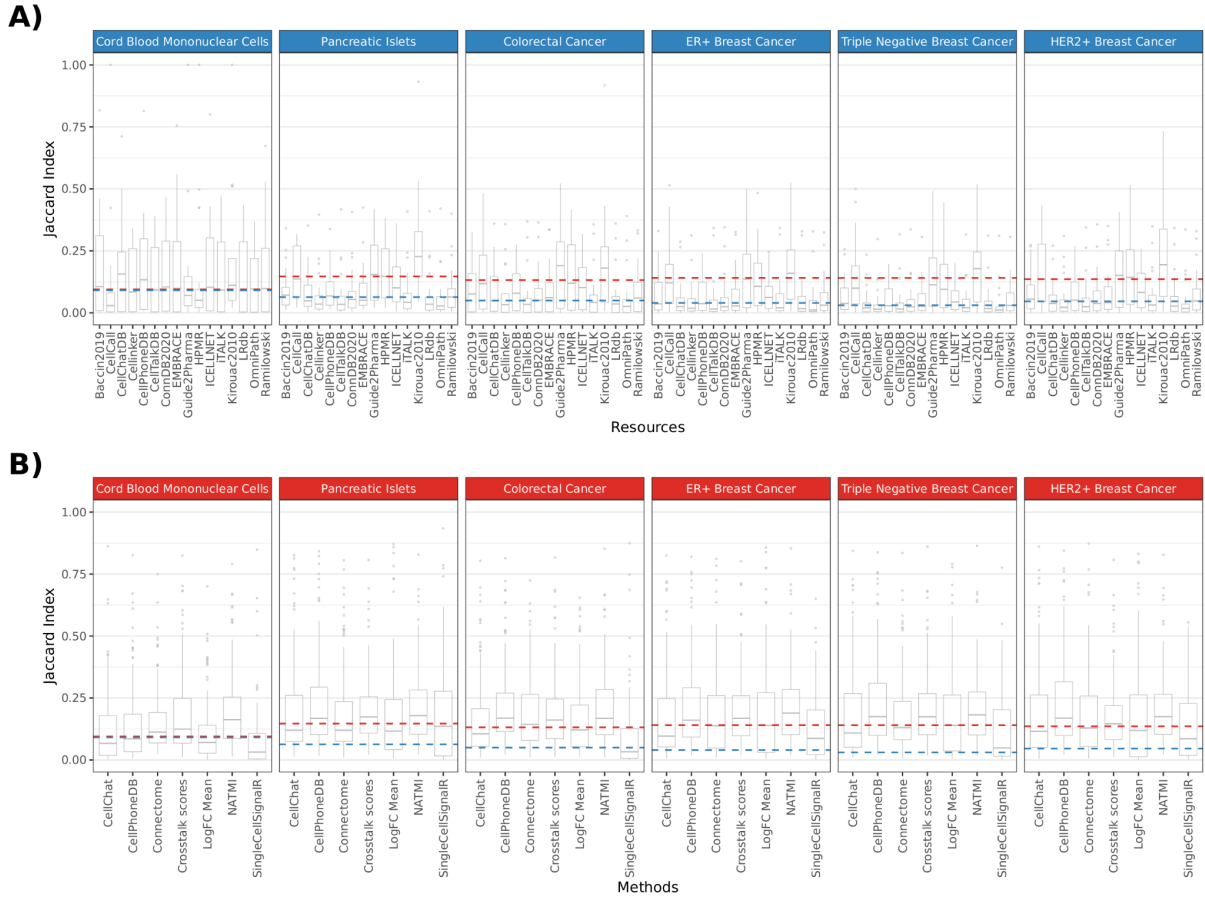
Supplementary Figure S16. Heatmap of median Jaccard index between the highest ranked 1,000 interactions per resource-method combination across all datasets. Clustered by Euclidean distance.



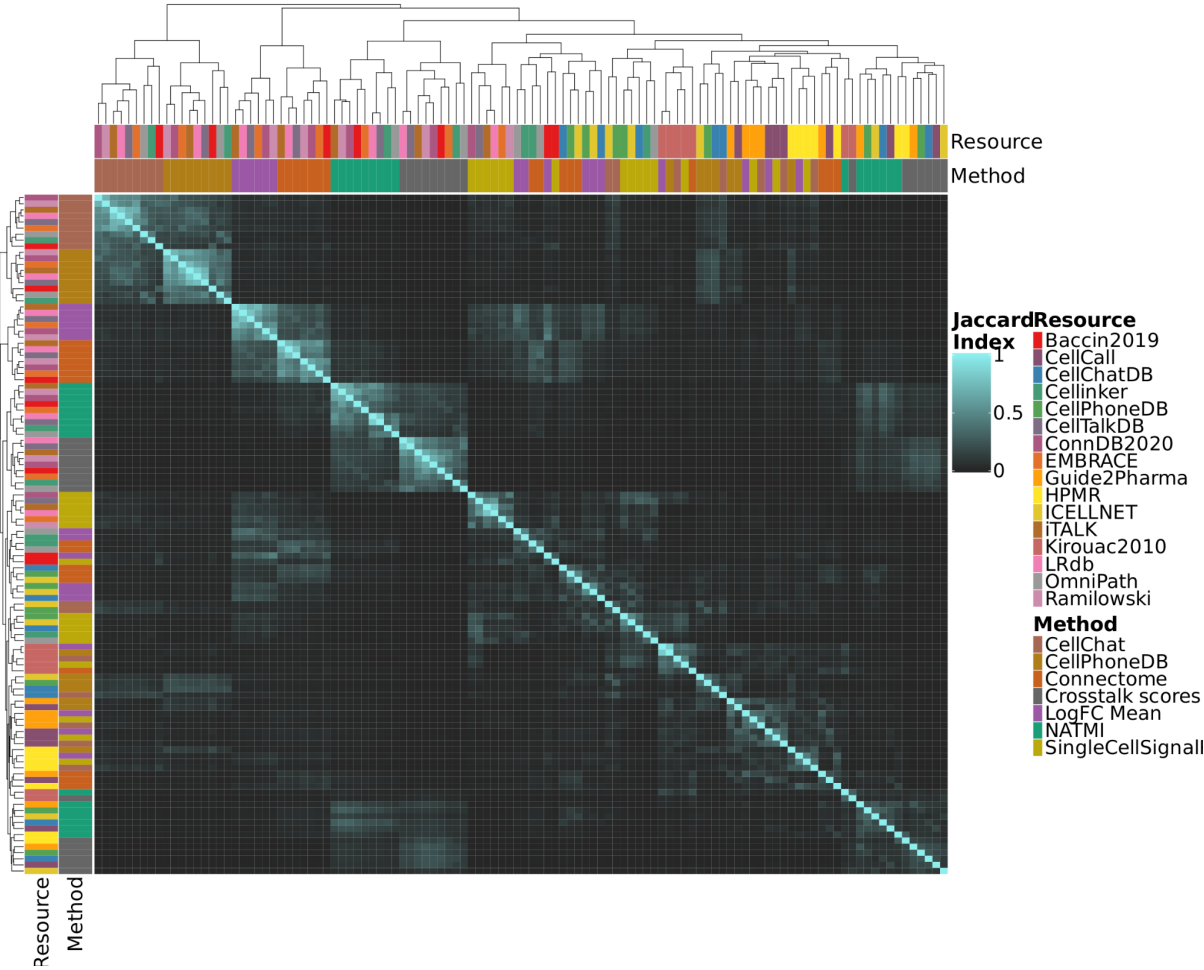
Supplementary Figure S17. Heatmap of median Jaccard index between the 1% highest ranked of interactions per resource-method combination across all datasets. Clustered by Euclidean distance.



Supplementary Figure S18. *Overlap (Jaccard index) in the 1,000 highest ranked A) when using the same Resource with different Methods (Blue; n=7) and B) when using the same Method with different Resources (Red; n=16). Boxplots represent the median pairwise jaccard index with hinges showing the first and third quartiles and whiskers extending 1.5 above and below the interquartile range; the lines overlap for the CMBCs dataset. Here, we use only the p-values for CellPhoneDB and CellChat, not their ‘composite’ scores (Supp. table 3).*

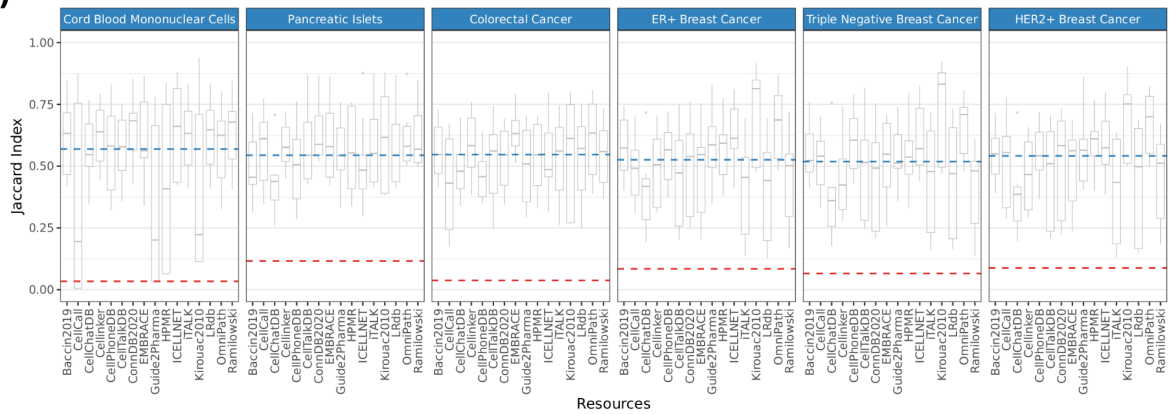


Supplementary Figure S19. Heatmap of median Jaccard index between the highest ranked 1,000 interactions per resource-method combination across all datasets when using only the *p*-values for CellPhoneDB and CellChat. Clustered by Euclidean distance (**Supp. table 3**).

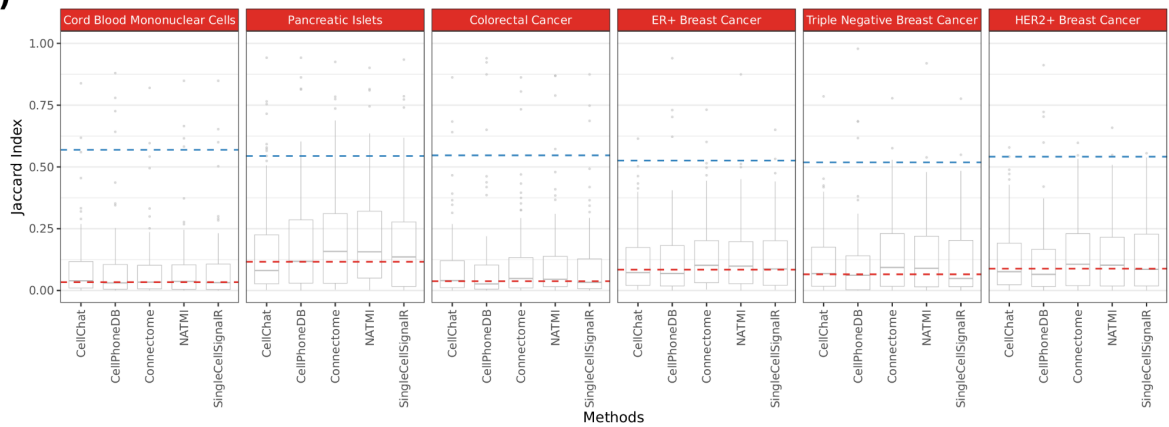


Supplementary Figure S20. Overlap (Jaccard index) in the 1,000 highest ranked, non-specific interactions A) when using the same Resource with different Methods (Blue; n=7) and B) when using the same Method with different Resources (Red; n=16). Boxplots represent the median pairwise jaccard index with hinges showing the first and third quartiles and whiskers extending 1.5 above and below the interquartile range. Here, we use non-specific scoring functions for each method, if available (Supp. table 3).

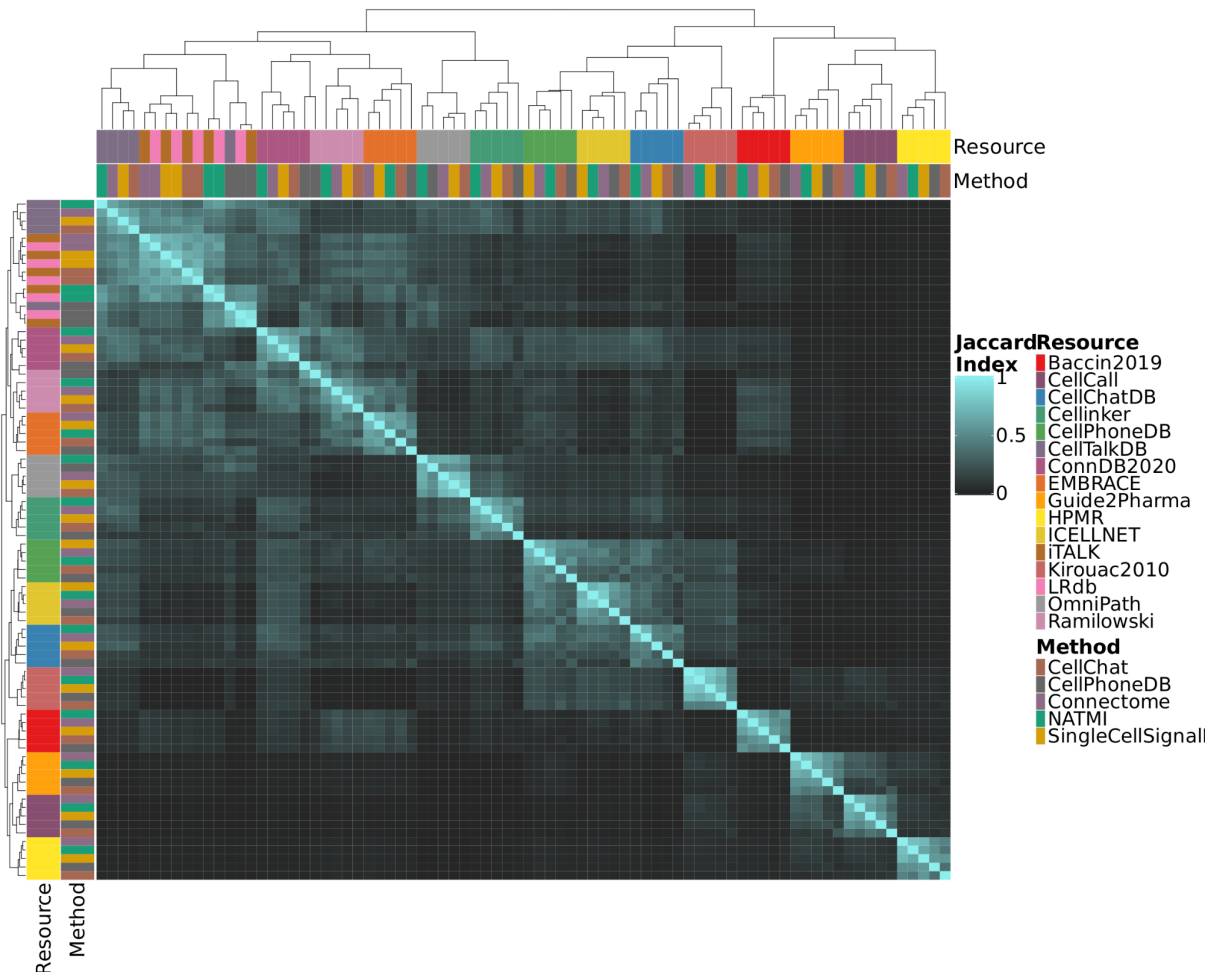
A)



B)



Supplementary Figure S21. Heatmap of median Jaccard index between the 1,000 highest ranked, non-specific interactions per resource-method combination across all datasets. Clustered by Euclidean distance.



Supplementary Figure S22. Relative frequencies of interactions per cell type estimated using the 1,000 highest ranked interactions for **A) CBMCs**, **B) Colorectal cancer**, **C) ER+ breast cancer**, **D) HER2+ breast cancer**, **E) Triple negative breast cancer**, and **F) Pancreatic Islet** datasets. The relative frequencies were defined as the number of interactions assigned to each cell type as ‘source’ or ‘target’ in the 1,000 highest ranked interactions.

A)



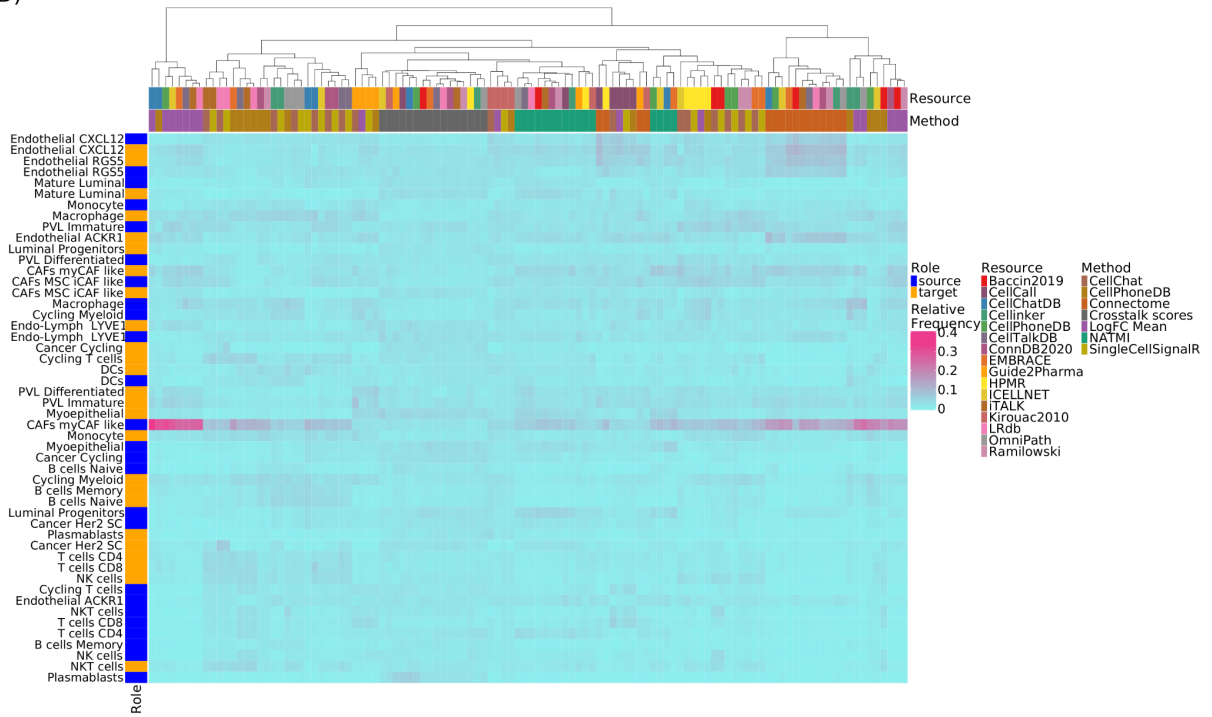
B)



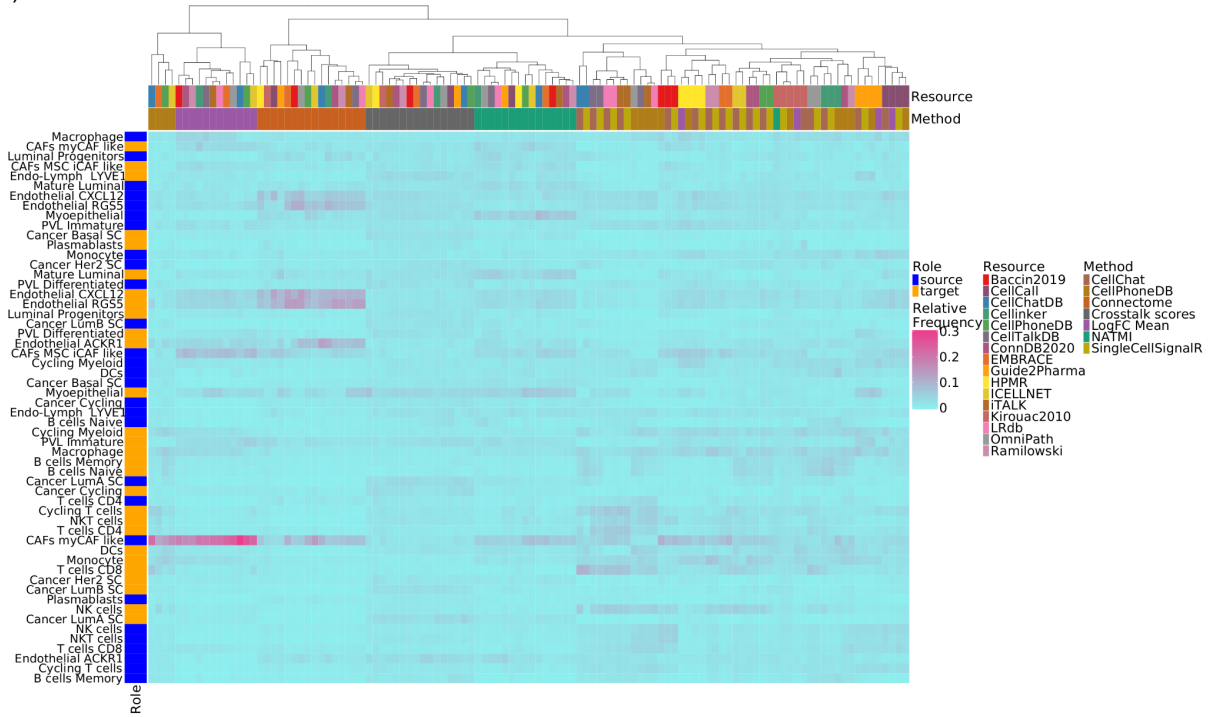
C)



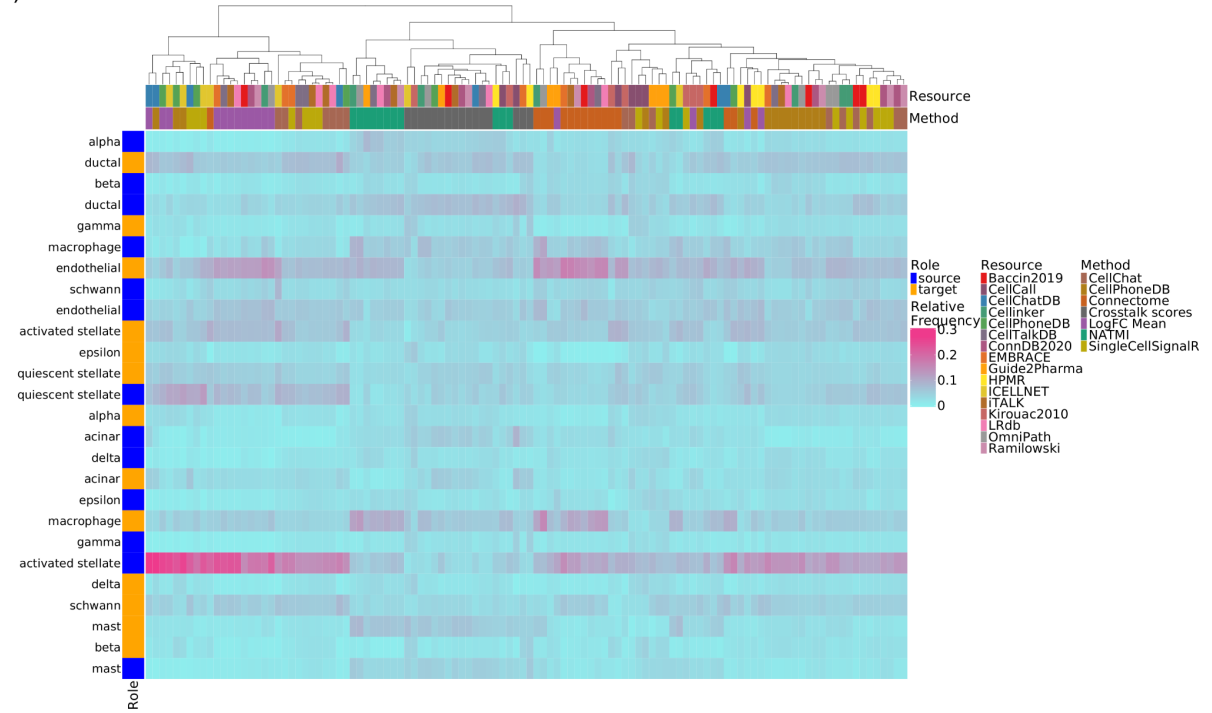
D)



E)

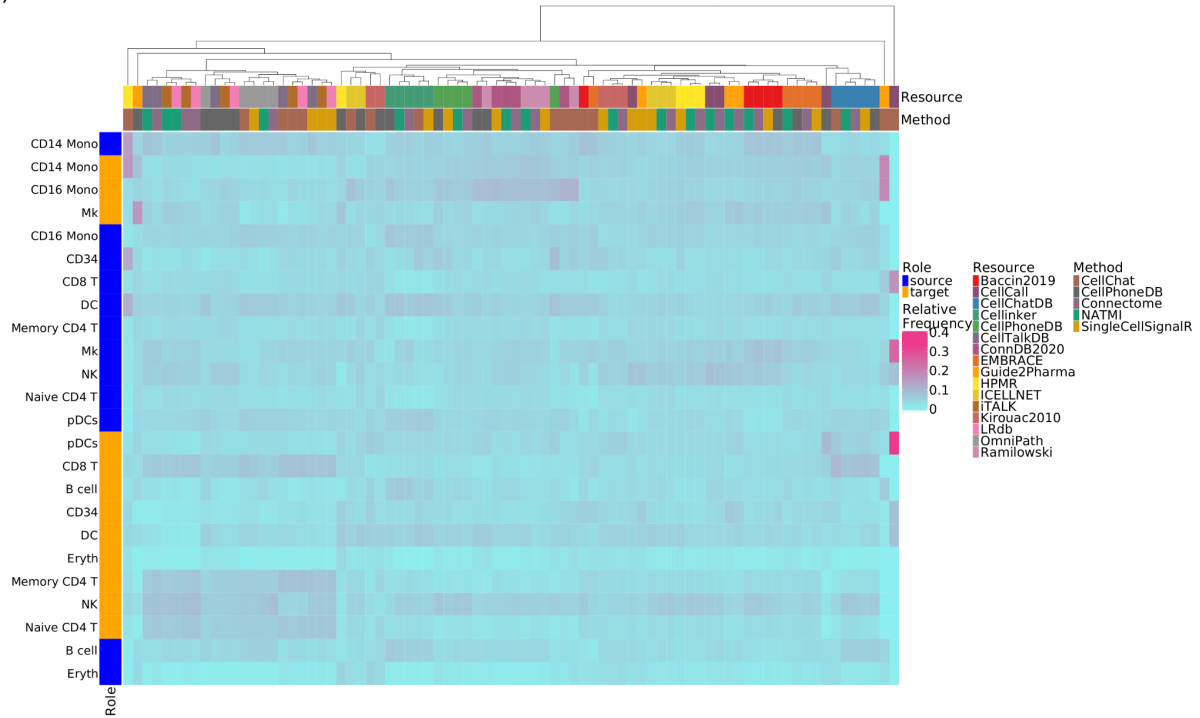


F)

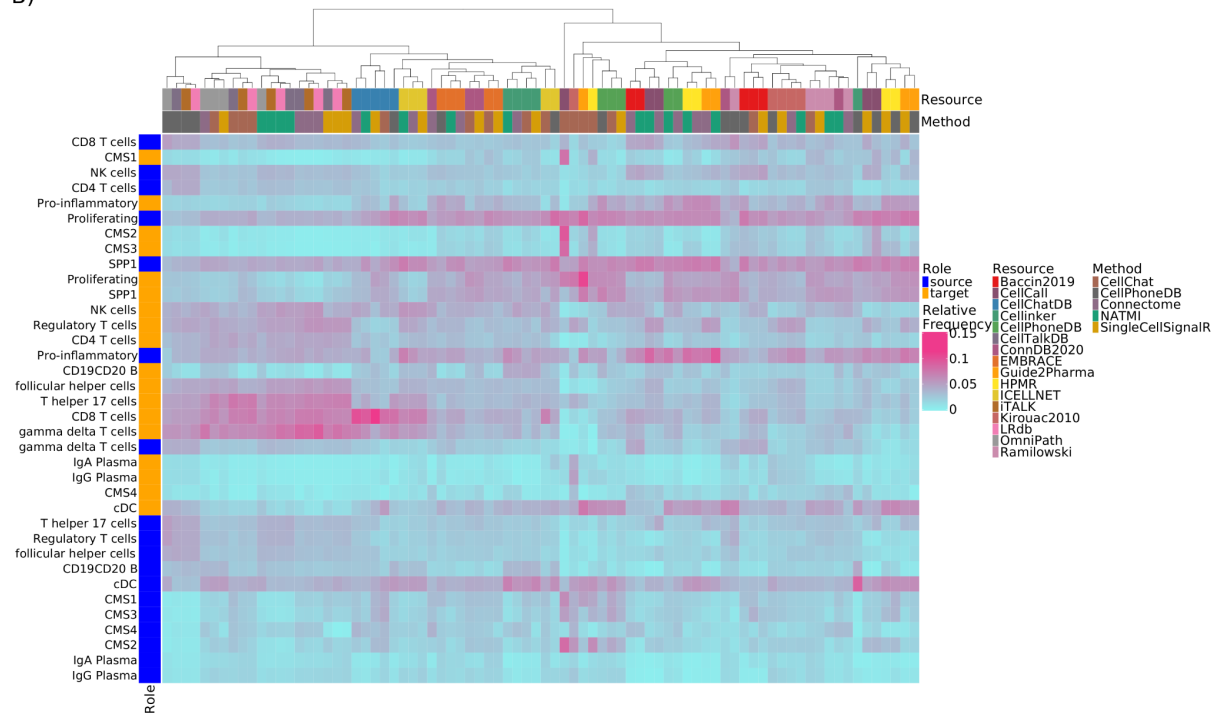


Supplementary Figure S23. Relative frequencies of interactions per cell type estimated using the 1,000 highest ranked, non-specific interactions for **A) CBMCs**, **B) Colorectal cancer**, **C) ER+ breast cancer**, **D) HER2+ breast cancer**, **E) Triple negative breast cancer**, and **F) Pancreatic Islet** datasets. The relative frequencies were defined as the number of interactions assigned to each cell type as 'source' or 'target' in the 1,000 highest ranked, non-specific interactions.

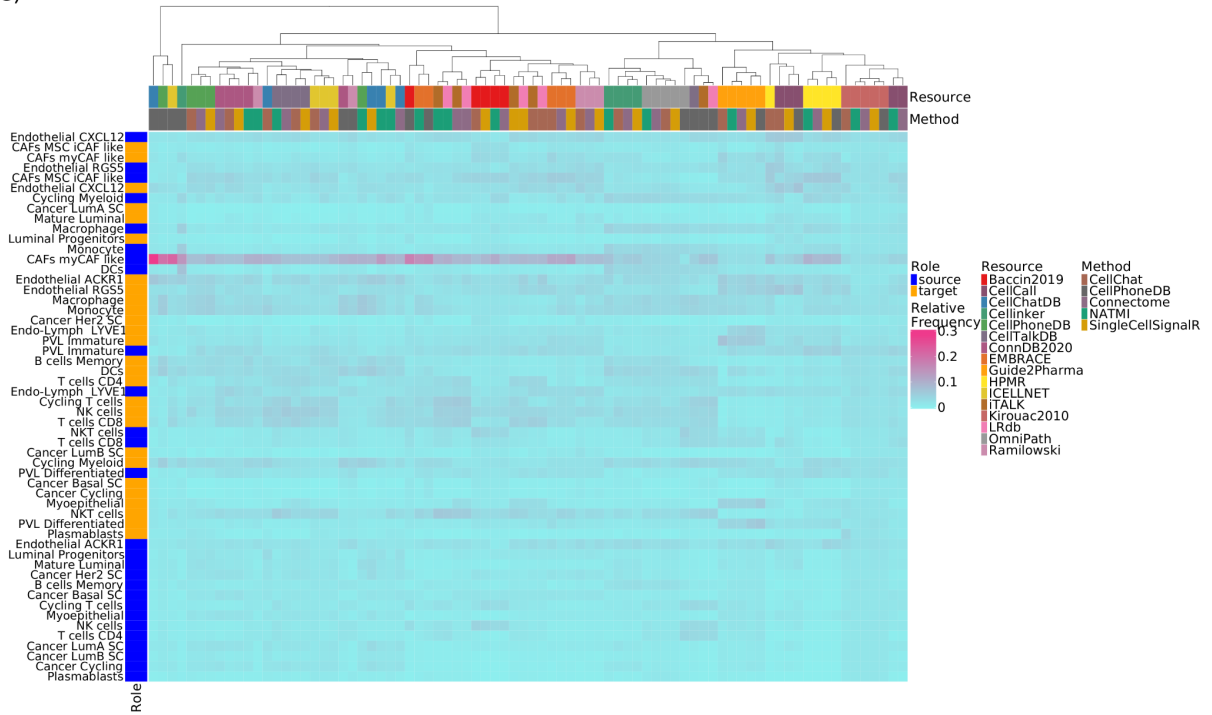
A)



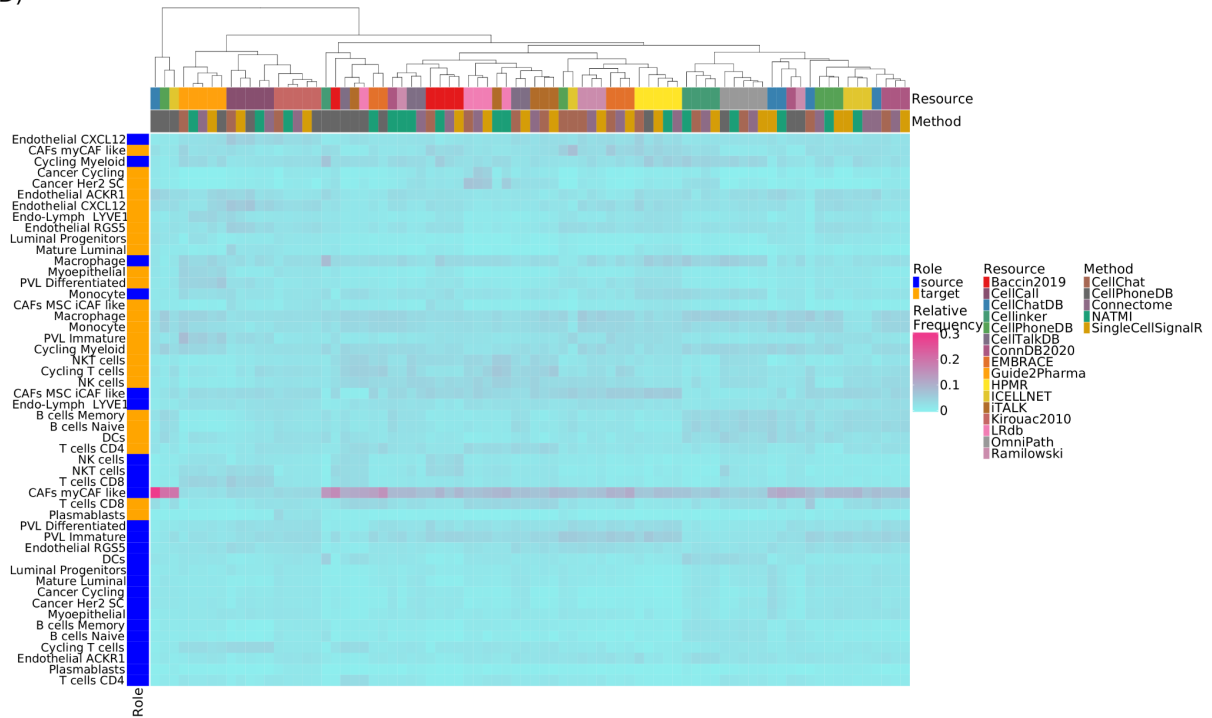
B)



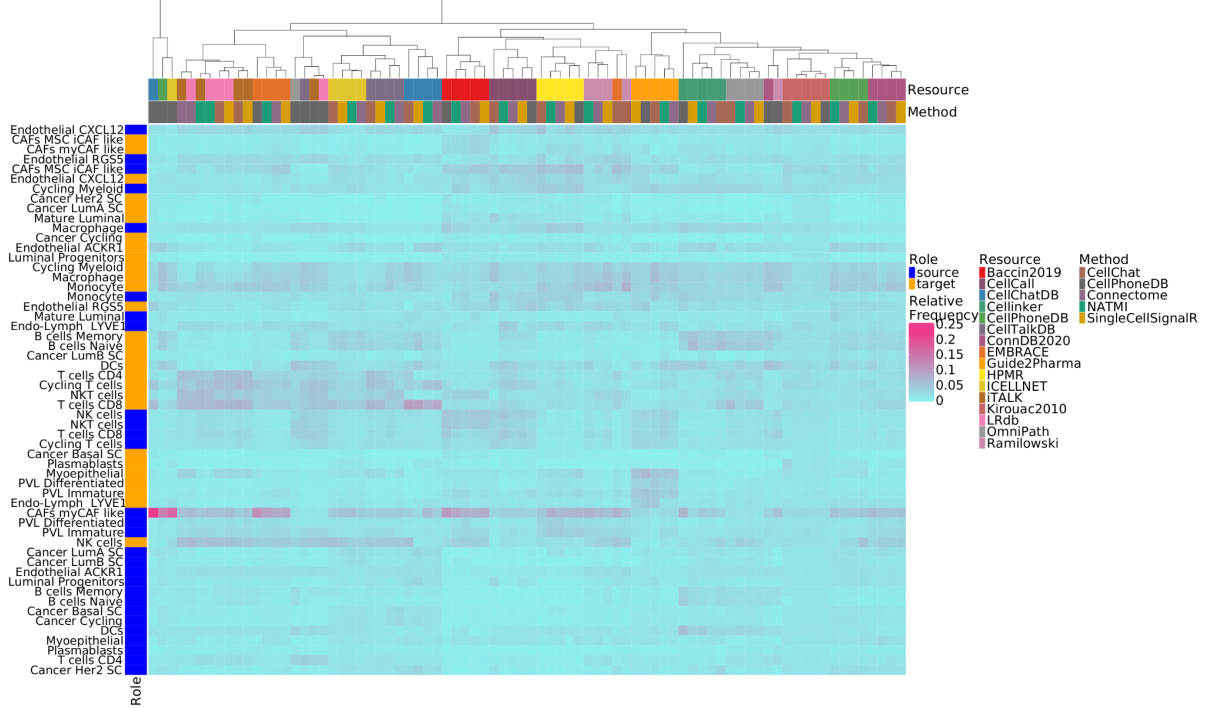
C)



D)



E)



F)



Supplementary Figure S24. Relative strength of interactions per cell type estimated using for A) CBMCs, B) Colorectal cancer, C) ER+ breast cancer, D) HER2+ breast cancer, E) Triple negative breast cancer, and F) Pancreatic Islet datasets.

A)



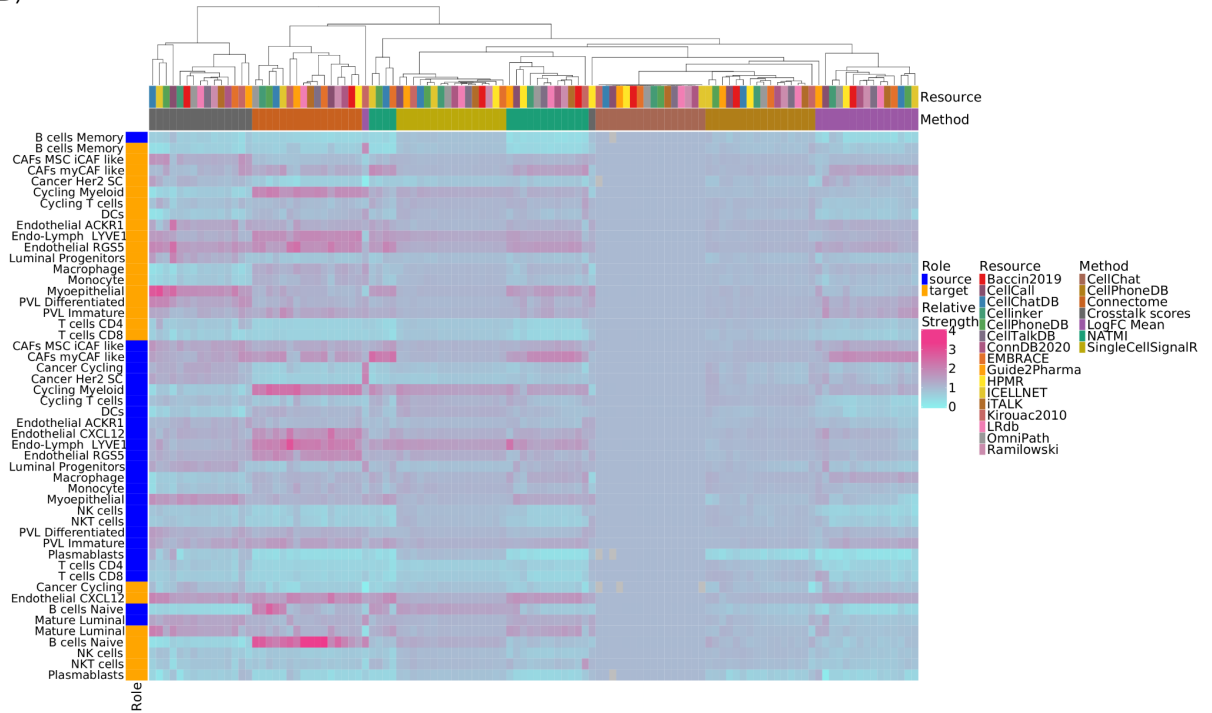
B)



C)



D)



E)



F)



Supplementary Figure S25. Relative strength of interactions per cell type estimated using the non-specific interaction scores for A) CBMCs, B) Colorectal cancer, C) ER+ breast cancer, D) HER2+ breast cancer, E) Triple negative breast cancer, and F) Pancreatic Islet datasets.

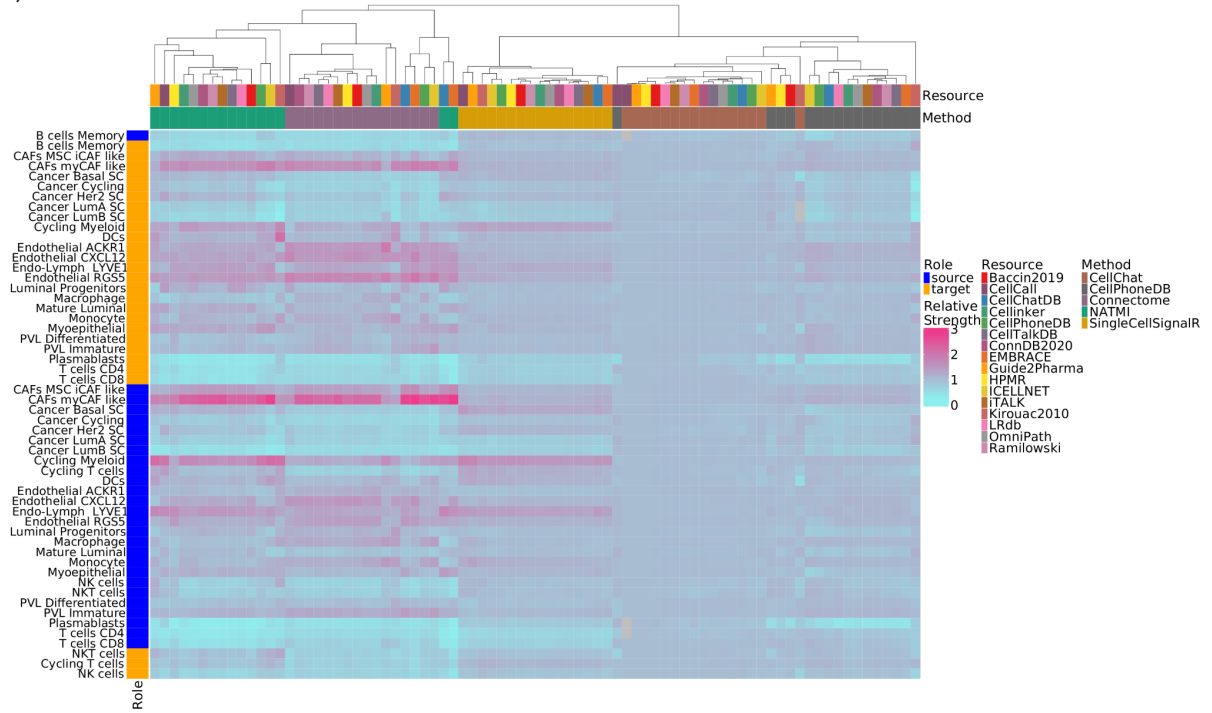
A)



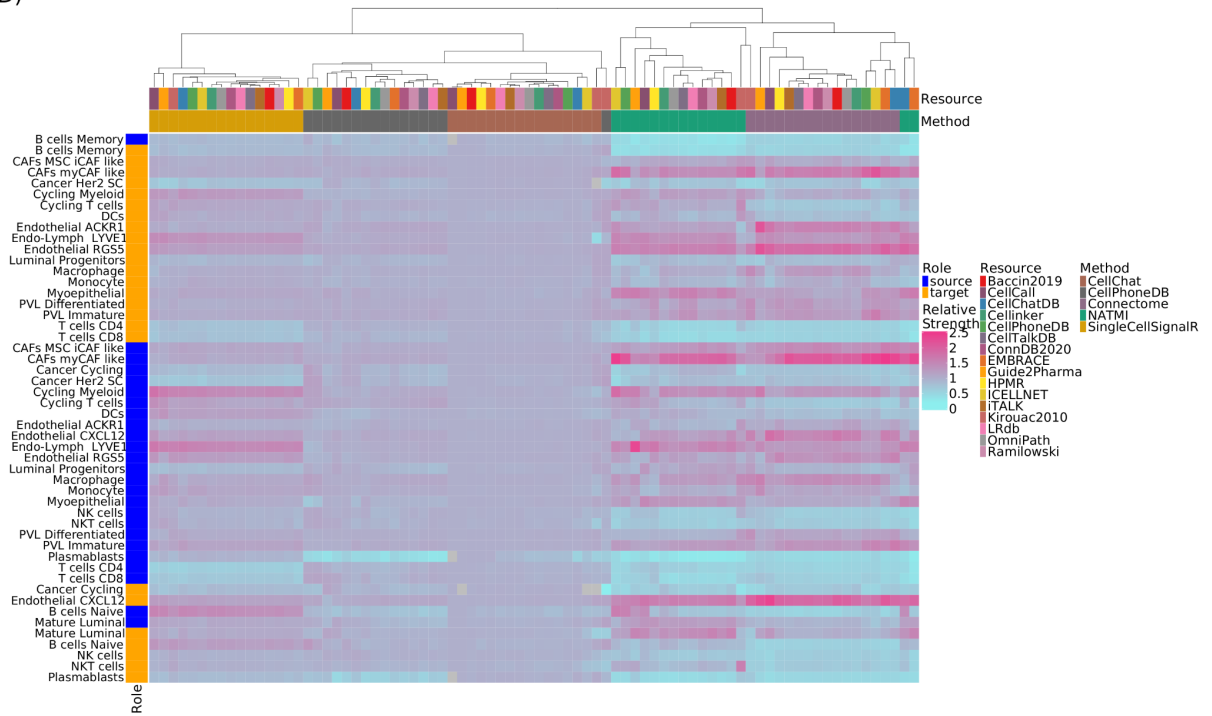
B)



C)



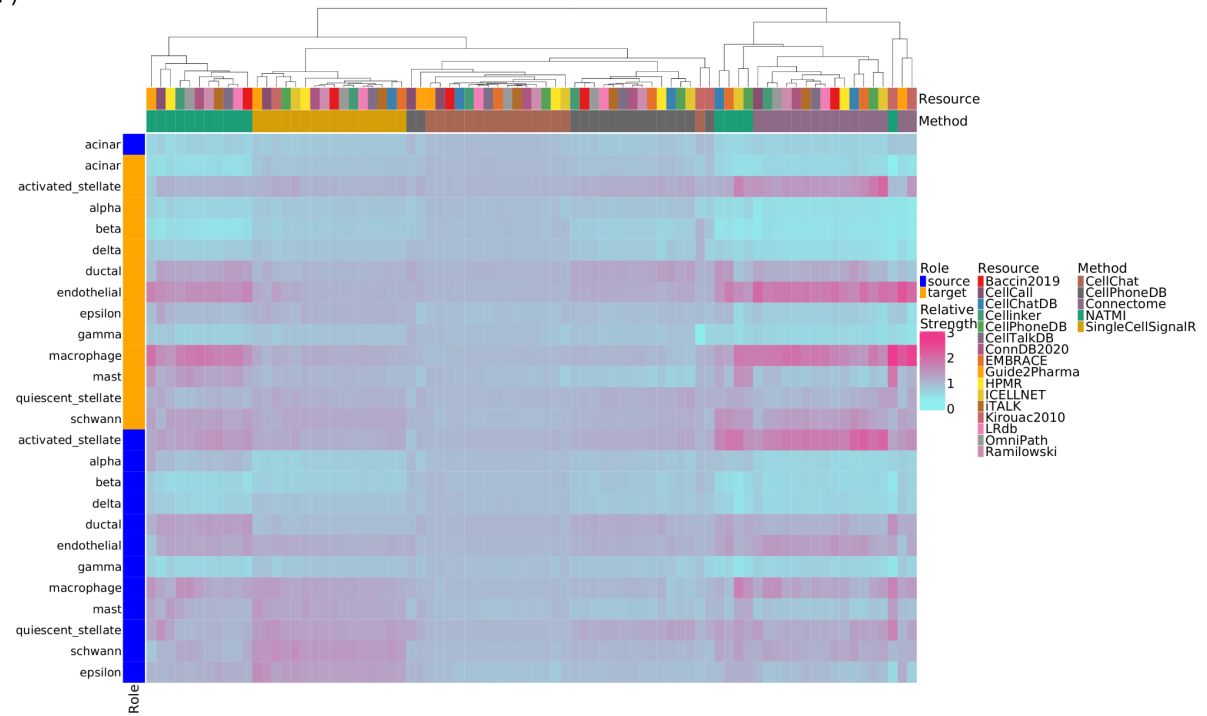
D)



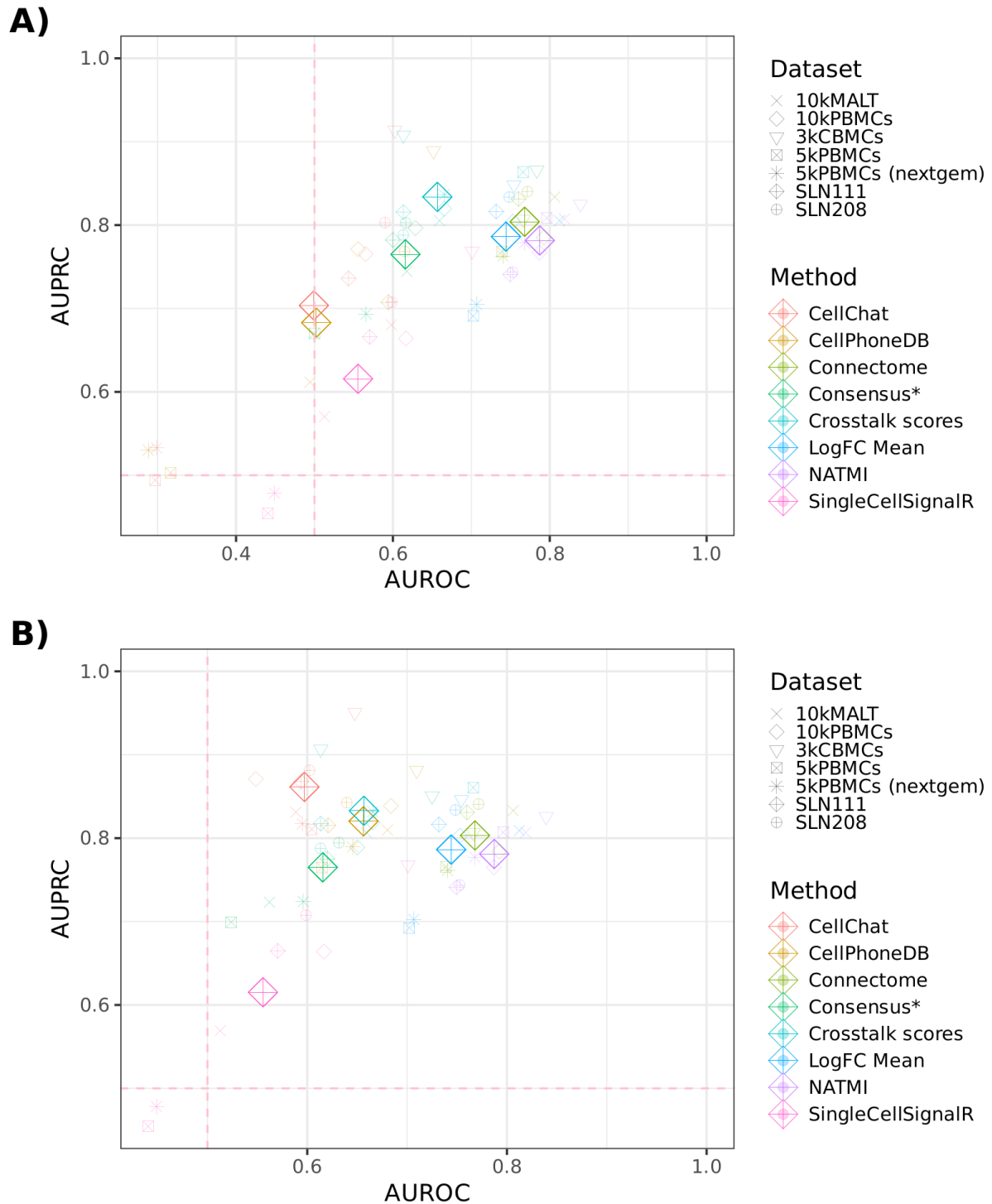
E)



F)



Supplementary Figure S26. Agreement with receptor protein specificity using **A) CellPhoneDB** and CellChat's composite scores, and **B) p-values** alone. Each method's performance was estimated independently, i.e. only using the interactions predicted following the preprocessing steps of each method.



Supplementary table 1. Unique Transmitters, Receivers, and interactions in each resource. We defined unique–interactions, receivers and transmitters between the CCC resources if they could be found in only one of the resources.

Resource	Transmitters	Receivers	Interactions
Baccin2019	5.71%	4.93%	10.60%
CellCall	1.81%	0.51%	3.14%
CellChatDB	4.25%	3.78%	20.76%
Cellinker	30.34%	24.93%	39.30%
CellPhoneDB	2.99%	6.94%	10.68%
CellTalkDB	2.94%	5.24%	5.53%
ConnDB2020	6.12%	3.51%	8.04%
EMBRACE	0.43%	0.00%	0.53%
GuidePharm	0.68%	0.41%	5.52%
HPMR	8.22%	12.75%	18.12%
ICELLNET	0.31%	0.40%	2.25%
iTALK	0.00%	0.00%	0.11%
Kirouac2010	4.20%	0.00%	10.53%
LRdb	0.75%	0.00%	1.51%
OmniPath	4.09%	3.95%	8.45%
Ramilowski	0.00%	0.00%	0.00%
Total	6.35%	5.74%	10.35%

Supplementary table 2. Cell-cell communication resources - additional information.

Resource	Further curation	Sources	Interactions*	Original curation † §	Overlap with curated set †§
Baccin2019/(a) ¹	Murine identifiers (only), Multimeric complexes	Ramilowski2015, KEGG REACTOME, Literature	1,625	No ‡	82%
CellCall ²	Multimeric complexes, murine identifiers, Interactions downstream transcription factors (from KEGG), transcription factor regulons.	ConnectomeDB2020, CellLinker, CellTalkDB, CellChatDB, STRING	1,123	No	51%
CellChatDB ³	Multimeric complexes, 229 signaling pathway families, agonists and antagonists, co-receptors, localisations, Murine identifiers	KEGG, Literature	1,912	Yes	84%
Cellinker ⁴	Multimeric complexes, murine identifiers, sMOL ligands, intercellular communication roles	DLRP, HPMR, CellPhoneDB, Guide2Pharma, Literature	3,701	Yes	71%
CellPhoneDB ⁵⁻⁷	Multimeric complexes, intercellular communication roles	Guide2Pharma, I2D, IntAct, UniProt, Literature, HPIDB	1,219	Yes	90%
CellTalkDB ⁸	Murine identifiers	STRING, Literature	3,392	Yes	100%
ConnectomeDB2020 ⁹	Intercellular communication roles	Ramilowski2015, CellphoneDB, Baccin2019, LRdb, ICELNET, Literature	2,266	Yes †	99%
EMBRACE(a) ¹⁰	Murine identifiers	Ramilowski2015	1,639	No	97%
Guide2Pharma(b) ¹¹	-	Literature	665	Yes	100%
HPMR ¹²	-	Literature	596	Yes	100%
ICELNET ¹³	Multimeric complexes, Signalling families, Cytokine-focus	<u>STRING</u> , <u>Ingenuity</u> , <u>BioGRID</u> , <u>Reactome</u> , CellPhoneDB	738	Yes	95%
iTALK ¹⁴	Ligand categories	Ramilowski2015, HPMR, Guide2Pharma, <u>Graeber2001</u> , <u>Griffith2014</u> , <u>Cameron2003</u> , <u>Zhou2017</u> , <u>Auslander2018</u>	2,566	No ‡	96%
Kirouac2010 ¹⁵	-	Literature, <u>COPE</u>	152	Yes	100%

LRdb ¹⁶	-	cellsignal.com, Ramilowski2015, Guide2Pharma, HPMR, HPRD, Reactome, UniProt, Literature	3,228	No‡	96%
Ramilowski2015 ¹⁷	-	DLRP, HPMR, IUPHAR, HPRD, STRING, Literature	1889	Yes†	99%
scConnect ¹⁸	-	Guide2Pharma	479	No	92%

Asterisk (*): All the resources above, except CellCall which was obtained directly via its Github page and converted to OmniPath format, were retrieved from the OmniPath database (<https://omnipathdb.org/>). Here, we show the number of human interactions for each CCC dedicated resource subsequent to dissociation of complexes into subunits.

Cross (†): Does the resource contain original expert curated data? Here *expert curated* (synonyms: manually- or literature curated) means only the interactions curated in the context of cell-cell communication. We assessed the curation contents based on the publications, webpages, software manuals and data files.

Star (★) We collected the curated interactions from all resources which contained any. Then for each resource we measured the overlap against the curated set. Many resources contribute to the curated set, or integrate other resources which are part of it, resulting in a bias in the overlaps.

Section sign (§) These columns aim to give insights on the status of curated CCC interactions, with limitations described in further footnotes. None of these attributes is an objective measure of the value or quality of the resources.

Double dagger (§): Unclear whether the resource contains original curation effort, insufficient information in the description of methods or in the data

Dagger (†): connectomeDB2020 is an updated edition of Ramilowski2015

(a) Translated from murine identifiers to human, which accounts for the lower number of obtained interactions.

(b) Kept only the unique human-annotated interactions between transmitter and receiver proteins.

Supplementary table 3. Description of the different scoring settings used to compare the methods presented in this work.

	Composite#		Non-composite	Non-Specific
Method	<i>Used throughout the main text</i>		<i>Specificity alone for CellChat and CellPhoneDB</i>	<i>Scores which do not incorporate cell-pair specificity in interaction predictions</i>
CellChat	Probability	(Filtered by p-value ≤ 0.05)	<u>p-values alone</u>	Probability
CellPhoneDBv2	Truncated Mean	(Filtered by p-value ≤ 0.05)	<u>p-values alone</u>	Truncated Mean
Connectome	weight_scale		weight_scale	weight_norm
Crosstalk Scores	Crosstalk score		Crosstalk score	-
logFC Mean	logFC Mean		logFC Mean	-
NATMI	Specificity-based edge weight		Specificity-based edge weight	Mean-expression edge weight
SingleCellSignalR	LRscore		LRscore	LRscore
Hashtag (#): Unless explicitly mentioned, we used the composite method settings.				

Supplementary table 4. Signalling category examples.

Signalling type	Transmitter	Transmitter symbol	Receiver	Receiver symbol	Resource
Direct-contact	Q9NQS3	NECTIN3	Q495A1	TIGIT	Cellinker
Direct-contact	P52803	EFNA5	P54764	EPHA4	Ramilowski
Direct-contact	Q9NT99	LRRC4B	Q6UXZ4	UNC5D	Cellinker
Direct-contact	P10321	HLA-C	P43632	KIR2DS4	Ramilowski
Direct-contact	Q14952	KIR2DS3	Q7Z3B1	NEGR1	Cellinker
Other	P21741	MDK	P18827	SDC1	Cellinker
Other	P01374	LTA	P19438	TNFRSF1A	OmniPath
Other	P21741	MDK	P18827	SDC1	CellChatDB
Other	P49763	PGF	P17948	FLT1	EMBRACE
Other	P06858	LPL	P13611	VCAN	Cellinker
Secreted	Q8IZJ0	IFNL2	Q08334	IL10RB	Ramilowski
Secreted	P00747	PLG	P05556	ITGB1	iTALK
Secreted	P56706	WNT7B	O75197	LRP5	Ramilowski
Secreted	P20062	TCN2	P21554	CNR1	iTALK
Secreted	P01303	NPY	Q9Y5X5	NPFFR2	ConnDB2020

Supplementary Note 1. Protein localisation to categorise CCC

To estimate the localisation distributions of transmitters and receivers as well as to categorise CCC interactions according to signalling categories we obtained protein subcellular localisation annotations via OmniPath¹⁹, which combines this information from 20 resources, such as UniProt, the Cell Surface Protein Atlas²⁰, and Membranome²¹. The localisation annotations were then filtered according to the 51st consensus percentile (**4.1. Methods**), and we used the localisations of transmitters and receivers to approximate the categories of interactions. The largest part of interactions were those between secreted proteins targeting transmembrane proteins (Secreted -> Transmembrane), which we refer to as the ‘Secreted signalling’ category. Further, we attributed interactions between and within the transmembrane and peripheral plasma membrane proteins (Transmembrane -> Transmembrane, Peripheral -> Transmembrane, Transmembrane -> Peripheral, Peripheral -> Peripheral) to intercellular signalling events that require physical contact between cells, or ‘Direct-contact’ signalling. Interactions categorised as neither secreted nor direct-contact were labelled as ‘Other’ and made up the remainder of the interactions. These were largely a consequence of the localisation annotation process, i.e. such involving proteins matched to multiple localisation categories; e.g. proteins annotated as both secreted and peripheral/transmembrane (**Supp. table 4**).

On average 77% of transmitters and 89% of receivers were annotated as secreted and transmembrane proteins, respectively (**Supp. Fig. S6E-F**). CCC resources were predominantly (73% on average) composed of interactions associated with secreted signalling, while direct-contact signalling constituted a substantially smaller (18% on average) proportion of interactions (**Supp. Fig. S6G**). The proportions of secreted and direct-contact signalling varied between resources, as some of them, such as Cellinker and OmniPath had an overrepresentation of direct-contact signalling when compared to the collective, while the opposite was noted for Guide to Pharmacology and Kirouac2010 (**Supp. Fig. S6A**).

Our results suggest that localisations of transmitters and receivers were largely uniformly distributed and that secreted signalling was predominant across all resources. Yet, differences were noted between the relative abundance of secreted and direct-contact signalling interactions.

Supplementary Note 2. Examining the Disagreement in CCC predictions

Since methods report the different total numbers of interactions, we also assessed the agreement by comparing the top 1% predicted interactions, and found low overlap between the different combinations. In this case, the results generated using different methods showed markedly lower overlap than those generated using different resources (Supp. Fig. S12). We then merged and clustered the results from all of the datasets, and found that highest ranked interactions were partly grouped by method (Supp. Fig. S16-17). There was nevertheless some, albeit limited, similarity between the predictions of CellChat, CellPhoneDB, and SingleCellSignalR; NATMI and Crosstalk scores; as well as between logFC Mean and Connectome (Supp. Fig. S16-17). Results were broadly comparable when considering only the p-values for the ranking of CellChat and CellPhoneDB to compare with the other methods (Supp. Fig. S18-19; Supp. table 3).

To better explain the low overlap between the methods, we first hypothesised that the observed discrepancies stem from the method's distinct approaches to prioritise the interactions, and in particular the approaches used to assign cell type specificity to the interactions. For methods that provide additional alternative non-specific scoring functions, we used those functions which consider the magnitude of expression alone to estimate the CCC predictions (Supp. table 3). In this case, the overlap between methods was substantially higher, ranging from 0.519 to 0.569 (median = 0.543), while the low overlap when using different resources remained relatively unchanged and ranged from 0.034 to 0.116 (median = 0.075) (Supp. Fig. S20) and there was a clear clustering by the different resources (Supp. Fig. S21).

We thus postulated that the low overlap between the methods when using their recommended scoring functions was explained by differences at the cell type level. As such, we calculated the frequencies of interactions per cell type, and saw grouping largely by method (Supp. Fig. S22). We performed the same analysis using the alternative, non-specific scoring functions and instead noted clustering by resource, while predictions from methods were generally grouped (Supp. Fig. S23). We also estimated the relative interaction strength assigned to

each cell type ([4.5 Methods](#)), and in this case we noted clustering by method for both the specific and non-specific interaction scores (**Supp. Fig. S24-25**).

The remainder of the differences between the top predictions across the different methods are expected to arise from the methods' distinct approaches in the preprocessing of the input data or from the fact that some methods consider multi-complex subunits whereas others omit such information.

Taken together, these results suggest that the low overlap between the methods when using their recommended scoring functions, is largely a product of the distinct approaches to compute the cell-type specificity aspect of the CCC interactions scores. Finally, this was also reflected by the relative importances assigned to the different cell types.

Supplementary Note 3. Agreement with Receptor Protein specificity

To assess the agreement between CCC predictions from transcriptomics data and antibody-tagged receptor protein abundance, we used seven CITE-Seq datasets ([Methods 4.8](#)), which had between 9 and 106 surface-protein genes matched to receptor proteins. In particular, we assessed the agreement of CCC methods with receptor protein specificity by estimating their area under the receiver-operator characteristic (AUROC) and area under the precision-recall curve (AUPRC) metrics ([Methods 4.6.3](#)).

We first built AUROC and AUPRC curves for each method using their independent universes, meaning that each method's performance was estimated using only the interactions returned by that method. While the methods' performance is not directly comparable, this allowed us to independently assess the performance of the methods as originally proposed.

All methods were better than random at predicting the most specifically expressed receptor proteins (**Supp. Fig. S26A**), including SingleCellSignalR, which does not explicitly take specificity into account. As anticipated, CellPhoneDB and CellChat showed markedly better performance when we used their p-values alone to predict receptor specificity instead of their composite scores (**Supp. table 3; Supp. Fig. S26B**).

Albeit one could assume that receptor protein abundance is possibly more informative about the occurring CCC events than RNA expression alone, the observed agreement of all methods with receptor specificity is itself largely expected due to the correlation between RNA and protein expression. Nevertheless, our analysis suggests that estimates of CCC events using RNA information are also expected to be a good proxy of predictions at the protein level.

Bibliography

1. Baccin, C. *et al.* Combined single-cell and spatial transcriptomics reveal the molecular, cellular and spatial bone marrow niche organization. *Nat. Cell Biol.* **22**, 38–48 (2020).
2. Zhang, Y. *et al.* CellCall: integrating paired ligand-receptor and transcription factor activities for cell-cell communication. *Nucleic Acids Res.* **49**, 8520–8534 (2021).
3. Jin, S. *et al.* Inference and analysis of cell-cell communication using CellChat. *Nat. Commun.* **12**, 1088 (2021).
4. Zhang, Y. *et al.* Cellinker: a platform of ligand-receptor interactions for intercellular communication analysis. *Bioinformatics* (2021) doi:10.1093/bioinformatics/btab036.
5. Garcia-Alonso, L. *et al.* Mapping the temporal and spatial dynamics of the human endometrium in vivo and in vitro. *BioRxiv* (2021) doi:10.1101/2021.01.02.425073.
6. Efremova, M., Vento-Tormo, M., Teichmann, S. A. & Vento-Tormo, R. CellPhoneDB: inferring cell-cell communication from combined expression of multi-subunit ligand-receptor complexes. *Nat. Protoc.* **15**, 1484–1506 (2020).
7. Vento-Tormo, R. *et al.* Single-cell reconstruction of the early maternal-fetal interface in humans. *Nature* **563**, 347–353 (2018).
8. Shao, X. *et al.* CellTalkDB: a manually curated database of ligand-receptor interactions in humans and mice. *Brief. Bioinformatics* **22**, (2021).
9. Hou, R., Denisenko, E., Ong, H. T., Ramilowski, J. A. & Forrest, A. R. R. Predicting cell-to-cell communication networks using NATMI. *Nat. Commun.* **11**, 5011 (2020).
10. Sheikh, B. N. *et al.* Systematic Identification of Cell-Cell Communication Networks in the Developing Brain. *iScience* **21**, 273–287 (2019).
11. Harding, S. D. *et al.* The IUPHAR/BPS Guide to PHARMACOLOGY in 2018: updates and expansion to encompass the new guide to IMMUNOPHARMACOLOGY. *Nucleic Acids Res.* **46**, D1091–D1106 (2018).
12. Ben-Shlomo, I., Yu Hsu, S., Rauch, R., Kowalski, H. W. & Hsueh, A. J. W. Signaling receptome: a genomic and evolutionary perspective of plasma membrane receptors involved in signal transduction. *Sci. STKE* **2003**, RE9 (2003).

13. Noël, F. *et al.* Dissection of intercellular communication using the transcriptome-based framework ICELLNET. *Nat. Commun.* **12**, 1089 (2021).
14. Wang, Y. *et al.* iTALK: an R Package to Characterize and Illustrate Intercellular Communication. *BioRxiv* (2019) doi:10.1101/507871.
15. Kirouac, D. C. *et al.* Dynamic interaction networks in a hierarchically organized tissue. *Mol. Syst. Biol.* **6**, 417 (2010).
16. Cabello-Aguilar, S. *et al.* SingleCellSignalR: inference of intercellular networks from single-cell transcriptomics. *Nucleic Acids Res.* **48**, e55 (2020).
17. Ramilowski, J. A. *et al.* A draft network of ligand-receptor-mediated multicellular signalling in human. *Nat. Commun.* **6**, 7866 (2015).
18. Jakobsson, J. E. T., Spjuth, O. & Lagerström, M. C. scConnect: a method for exploratory analysis of cell-cell communication based on single cell RNA sequencing data. *Bioinformatics* (2021) doi:10.1093/bioinformatics/btab245.
19. Türei, D. *et al.* Integrated intra- and intercellular signaling knowledge for multicellular omics analysis. *Mol. Syst. Biol.* **17**, e9923 (2021).
20. Bausch-Fluck, D. *et al.* A mass spectrometric-derived cell surface protein atlas. *PLoS ONE* **10**, e0121314 (2015).
21. Lomize, A. L., Lomize, M. A., Krolicki, S. R. & Pogozheva, I. D. Membranome: a database for proteome-wide analysis of single-pass membrane proteins. *Nucleic Acids Res.* **45**, D250–D255 (2017).